THESIS

DETERMING THE EFFICACY OF POLOXAMER 188 (P188) IN MENISCAL DAMAGE PREVENTION

Submitted by

Katherine Remley

Graduate Degree Program in Bioengineering

In partial fulfillment of the requirements

For the Degree of Master of Science

Colorado State University

Fort Collins, Colorado

Summer 2016

Master's Committee:

Advisor: Tammy Donahue

Sue James
Jeremiah Easley

Copyright by Katherine Remley 2016

All Rights Reserved

ABSTRACT

DETERMING THE EFFICACY OF POLOXAMER 188 (P188) IN MENISCAL DAMAGE PREVENTION

Meniscal injuries compose 15% of all knee injuries, most often sports-related. Due to the meniscus's avascular nature, healing is difficult and injury often results in a partial meniscectomy. Research has shown meniscectomies drastically decrease contact area between the femur and tibia and increase strains experienced by the meniscus. This additional strain predisposes the knee to developing post-traumatic osteoarthritis. Poloxamer 188 (P188) is a non-ionic, amphillic surfactant that may have the ability to prevent cell death through selective insertion into the cell membrane. This in turn may prevent damaged cell signaling and reduce overall tissue degradation. While P188 has been studied and shown promise in mitigating cell death in cartilage, the effects of P188 on the meniscus are unknown. To investigate the effects of P188 on the meniscus, the goals of this project were to: 1) create a user friendly graphical user interface for a custom bioreactor capable of displacement control for precise loading of meniscal explants to physiological and supraphysiological strains; 2) determine the efficacy of P188 in mitigating meniscal tissue damage through cell viability, mechanical data and histological analysis.

ACKNOWEDGEMENTS

First of all, I would like to thank my advisor Dr. Tammy Donahue for all her guidance and patience over the past two years. This project could not have been completed without her support and encouragement. She was an integral part of this project and I am extremely grateful for her constant willingness to answer my many questions. I am also grateful to my committee, Dr. Sue James and Dr. Jeremiah Easley, for taking the time to review my thesis and offer valuable suggestions.

I would also like to thank all my lab members: Kristine, Hannah, Ben, and Brett. I am so grateful for all their help over my two years here at CSU. They helped create a great working environment and were always there to offer their support from helping perform experiments in the lab to providing feedback on oral presentations.

My family has also been a great source of support. Thanks for constantly encouraging me to pursue my master's degree. I could not have done it without them.

TABLE OF CONTENTS

CHAPTER 1: INTRODUCTION

1.1 Knee Joint Gross Anatomy

Acting as a modified hinge, the knee is the largest joint in the body. It is comprised of the femorotibial joint and the patellofemoral joint. The patellofemoral joint consists of the articulation between the patella and femoral trochlea and provides knee stability. The attachment of the quadriceps to the patella increases the moment arm and reduces the necessary force for knee extension [1,5]. The focus of this study lies within the femorotibial joint, in which the femur articulates with the tibia. The distal part of the femur consists of two rounded condyles, which interact with the mostly flat tibial plateau [2]. The basic components of the femorotibial joint can be seen in the image below (Figure 1.1).

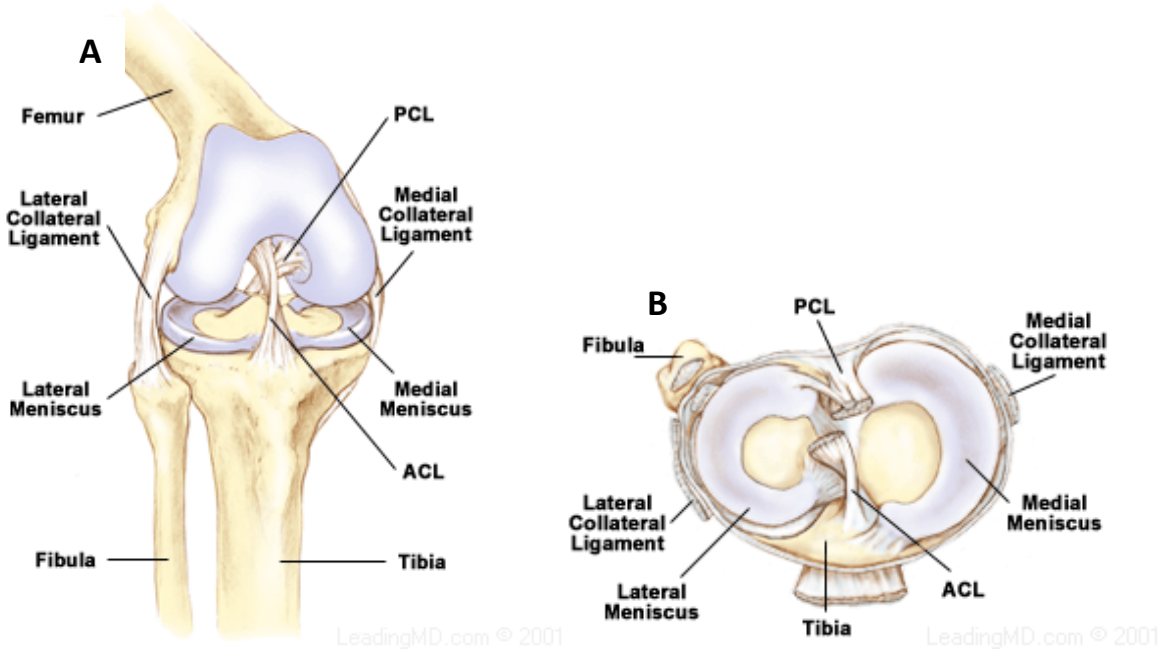

Figure 1.1. A) Anterior view of human knee B) Superior view of human knee
Images from: http://www.leadingmd.com/patientEd/meniscus/overview.asp

Two wedge shaped menisci, lateral and medial, ease this incongruity in shape improving joint contact. Semicircular in shape, the medial meniscus has a wider posterior horn than anterior horn. The anterior and posterior horns are attached to the tibial plateau by insertional ligaments. The anterior horn attaches to the intercondylar fossa in front of the anterior cruciate ligament (ACL) and the posterior fibers of the anterior horn meld with the transverse intermensical ligament. This ligament connects the anterior horns of the lateral and medial meniscus. The posterior horn of the medial meniscus is anchored to the posterior intercondylar fossa of the tibia between the posterior insertional ligament of the lateral mensicus and the posterior cruciate ligament (PCL). Marginally, the medial meniscus is connected to the joint capsule along its entire length. Midway the meniscus blends with the deep medial collateral ligament fastening it to both the femur and tibia [1].

The lateral meniscus is circular in form and overlays a larger portion of the tibial plateau compared to the medial meniscus. Unlike the medial meniscus the anterior and posterior horns of the lateral meniscus are similar in width. The anterior insertional ligament of the lateral meniscus embeds into the intercondylar fossa of the tibia and partially blends with the ACL [3,4]. The posterior horn of the lateral meniscus is more complex. It attaches behind the lateral intercondylar eminence and in front of the posterior insertion of the medial meniscus. However, in some instances the posterior insertional ligament splits and attaches to the intercondylar fossa of the medial femoral condyle. The insertional ligaments are known as the meniscofemoral ligaments and depending on the location of insertion into the femoral condyle are known as the ligament of Humphrey, anterior to PCL, or Wrisberg, posterior to PCL [1,4,6]. According to Kohn and Moreno, 76% of the knees examined had the Wrisberg ligament and

37% had the Humphrey ligament present in at least one knee. The percentage of these ligaments occurring in both the right and left knee were considerably lower, 57% of donors had the Wrisberg ligament present and 26% had the Humphrey ligament present [3]. Marginally, the lateral meniscus is loosely attached to the joint capsule. Unlike the medial meniscus, the lateral meniscus does not attach to a ligament at its midway point, allowing the lateral meniscus greater translation [1].

Other major structures within the knee joint include the cruciate and collateral ligaments. There are two cruciate ligaments, the anterior cruciate ligament (ACL) and posterior cruciate ligament (PCL), which as the name suggests form a cross. The ACL is anchored to the posterior of the medial surface of the lateral condyle and travels down to the tibia to attach in front of and lateral to the medial tibial spine. Its primary purpose is to restrict anterior translation of the tibia on the femur. Secondary responsibilities also include limiting internal rotation, varus, valgus and hyperextension. The PCL attaches to the lateral surface of the medial condyle and inserts into the tibia in the depression between plateaus. Its principal function is to prevent posterior translation of the tibia on the femur, but also regulates varus, valgus and external rotation [1].

The collateral ligaments run vertically on the medial and lateral sides of the knee. The medial collateral ligament (MCL) begins at the medial femoral epicondyle and extends downs to the tibia. It resists valgus rotation, external rotation and straight medial and lateral translation of the tibia. From a fovea posterior to the lateral epicondyle, the lateral collateral ligament (LCL) extends down to the fibular head with its primary function being resistance to varus motion[1].

1.2 Meniscus Structure and Function

The principal components of the extracellular matrix (ECM) of the meniscus are water, collagen, proteoglycans and glycoproteins. The meniscus is largely hydrated containing approximately 74% water [7]. Of the dry weight, collagen makes up 75%, proteoglycans 17% and glycoproteins and elastin less than 1%. Type I collagen is most prevalent, but Type II, III, V and VI are also found throughout the meniscus [8].

Petersen and Tillman found there were three distinct layers of collagen using scanning electron microscopy [9]. On the tibial and femoral surfaces, there is a thin superficial layer which consists of a mesh of fine collagen fibrils. Beneath this on both the tibial and femoral faces there is a lamellar layer. This layer is approximately 150-200 um thick and is comprised of small lamellar bundles that have a random orientation on the tibial surface and a radial orientation on the femoral surface. In the central main layer, larger bundles of collagen fibrils run circumferentially giving the meniscus the ability to transfer loads through the joint. While the large majority of fibers run circumferentially, there are a few radial “tie” fibers interwoven within the circumferential fiber bundles. These “tie” fibers supply structural support and prevent longitudinal splitting [9,10]. While studying bovine meniscus Cheung found regional distributions of type I and II collagen fibers. The outer two-thirds consisted primarily of type I collagen while the inner one third was largely made of type II collagen. Trace amounts of type III and V collagen were present as well [11].

Proteoglycans consist of a protein backbone to which glycosaminoglycan (GAGs) chains are covalently bonded. GAGs are negatively charged and associate with sodium ions which can in

turn associate with water. The presence of water in the meniscus confers its compressive abilities. In the human meniscus the percent GAGs are 40% chondroitin 6-sulfate, 10-20% chondroitin 4-sulfate, 20-30% dermatan sulfate and 15% keratin sulfate. Two types of proteoglycans have been documented in the meniscus. Aggrecan, a large proteoglycan, binds to hyaluronic acid creating proteoglycan aggregates. These aggregates are formed when several proteoglycans bind to hyaluronic acid with the help of link proteins. The other type of proteoglycan is small and non-aggregating with only one or two chains of dermatan or chondroitin sulfate attached [10,12,13].

Also present in the ECM are glycoproteins. Several of these serve as an adhesive, binding to other matrix molecules or cells. They serve an important function acting as molecular glue and providing methods for cell migration and attachment. These include type VI collagen, fibronectin, and thrombospondin [13]. Small concentrations of elastin have been detected in the meniscus as well. However, its exact function is yet to be determined [8].

The menisci are key to a properly functioning knee joint as they deform and move with flexion and extension of the knee allowing the tibia and femur to remain in congruity. From 0-120 degrees of flexion, anterior-posterior translation of the medial meniscus is approximately 5 mm while the lateral meniscus experiences twice that with approximately 11 mm of movement. The medial meniscus periphery blends with the MCL and is therefore more confined. In rotation the lateral meniscus has more freedom to move while the medial meniscus is again restricted by the MCL. This leads to an increased risk of tear in the medial meniscus[10].

The meniscus is a biphasic viscoelastic material due to its fluid and solid phase. The fluid phase makes up 74% of the wet weight and is composed of water and interstitial electrolytes. Collagen, proteoglycans and other noncollagenous proteins form the solid phase consisting of 26% of the wet weight. This solid phase acts as a permeable fiber-reinforced composite [19]. As the joint is loaded, a tensile or hoop stress develops in the circumferentially oriented collagen fibers. The meniscal horn attachments prevent the meniscus from being extruded from the joint as load increases. The importance of this hoop stress has been demonstrated in various studies [19,20,22]. Full radial tears, which disrupt the circumferential fiber arrangement, lead to loss of tensile strength and equate to a total meniscectomy in load transfer [20,22]. The mechanical response can be separated into two phases, the initial elastic response and the time-dependent fluid flow. As the knee joint is loaded, the solid matrix and interstitial fluid of the meniscus are compressed increasing its hydrostatic pressure. After the initial compression, stress relaxation occurs as the fluid flows out of the meniscus lowering the hydrostatic pressure. Fluid flow persists until pressure equilibrium is achieved [21].

Besides its biphasic properties, the meniscus is also transversely isotropic. Leslie et al performed a study to evaluate the response of the meniscus in the axial, radial and circumferential directions in unconfined compression [23]. The tissue showed higher stiffness values under axial compression compared to loads applied in the radial and circumferential directions. At high strain rates (80%), the Young's modulus in the axial direction was 299 MPa, while the radial and circumferential directions showed no significant differences with modulus' of 287 and 288 MPa respectively [23]. Further studies have explored regional variation within the menisci. A study by Jones et al focused on hoop strains in the medial meniscus under

compression. The anterior and center portions had similar mean strains of 2.86% and 2.65% respectively, while the posterior section displayed significantly lower strains with a mean of 1.54% [22]. A 2009 study by Bursac et al further elicited the regional variation in the human meniscus [58]. The medial meniscus showed significantly higher compressive stiffness in the anterior segment compared to the central and posterior segments. The anterior region of the medial meniscus was also significantly stiffer than the anterior region of the lateral meniscus. The lateral meniscus showed no significant differences in regional stiffness values, but there was a general increase moving from the anterior to posterior segments. This difference in modulus values positively correlated with GAG content. The anterior segment of the medial meniscus had higher GAG content than the central and posterior segments as well as the anterior segment of the lateral meniscus. Higher GAG content produces larger swelling pressures which better allow the menisci to resist compression.

The menisci serve several functional roles including load bearing, shock absorption, joint stability and proprioception [4]. The meniscus was originally thought to be a vestigial organ which served no real purpose. Until 1948 when Fairbank demonstrated the degenerative effects of a meniscectomy, it was common practice to remove the entire structure in the event of injury [14]. Depending on degree of flexion of the knee, 50-85% of the load is transferred through the menisci [10]. Meniscectomy greatly decreases the joint's ability to transmit loads as the contact area is decreased and the contact force increases. Kurosawa et al showed that after total meniscectomy the contact area was reduced by a third to half. This resulted in 2-3 times increased contact forces [15]. Lee et al demonstrated the effects of partial and total medial meniscectomy. With a decreased contact area of 20% (50% meniscectomy), the peak

contact stress increased by 43% while a decreased contact area of 54% (total meniscectomy) resulted in a peak contact stress increase of 136% [16].

Hoshino and Wallace examined the impact absorbing ability of the knee joint by subsequently removing soft tissue and subchondral bone [47]. Removing only the meniscus increased the mean peak force within the joint by 20%. Voloshin and Wosk performed a study measuring shock absorption using accelerometers and claimed a 20% reduction in the joint's shock absorption ability with a total meniscectomy [17]. However, Andrews et al. dispute Voloshin and Wosk's findings, stating the menisci may not have caused the decrease in shock absorption as painful knees with intact menisci also showed the same loss of shock absorption [18].

The meniscus is also a well-known secondary stabilizer in the knee joint. Primary resistance to anterior tibial translation is provided by the ACL. A 1982 study by Levy et al demonstrated the meniscus's secondary role in joint stabilization. In knees that had undergone a total meniscectomy, but still had an intact ACL there was no change in anterior-posterior displacement compared to an intact knee. However, after sectioning of the ACL, the medial meniscus resisted anterior-posterior displacement significantly compared to a knee lacking both the medial meniscus and ACL [24]. A study by Shoemaker and Markolf reinforced these results and highlighted the particular importance of the posterior horn of the medial meniscus in resisting anterior tibial force [25]. A later study by Levy et al focused on the effect of lateral meniscectomy on anterior and posterior translation on the knee. Results indicated that the lateral meniscectomy did not provide the same wedging effect and did not prevent anterior translation in the ACL deficient knee [26]. A more recent study by Musahl et al indicated that

while the lateral meniscus may not play a part in resisting anterior-posterior displacement from anteriorly directed loads on the tibia, it may resist anterior tibial translation during a pivot movement. During a pivot, the knee undergoes valgus and rotary loads [27].

It has also been suggested that the meniscus may play some role in proprioception. Aagaard proposed this as a possibility due to the neurophysiology of meniscal tissue [21]. The nerve branches are found in the same outer third region of the meniscus as the blood supply with the horns containing the largest number of fibers. Three different types of nerve endings have been recognized within meniscal tissue: Pacini corpuscles, Ruffini endings, and Golgi tendon organs. The existence of these mechanoreceptors in the menisci suggest an essential role in nerve transmission. Aagaard suggests that neural information from these mechanoreceptors may moderate the anterior-posterior translation of the femoral condyle on the tibial plateau [21].

1.3 Cellularity

In the early formation stage, meniscus tissue consists mostly of rounded cells compacted together [29]. With maturation comes cell differentiation. Three distinct types of cells have thus far been identified in a fully mature meniscus. These are superficial zone cells, round or oval-shaped fibrochondrocytes and fibroblast-like cells. The superficial zone cells lie just below the surface of the tissue and have a fusiform shape with no cytoplasmic projections. Fibrochondrocytes, round or oval-shaped, are found in the middle and inner portions of the meniscus and have a pericellular matrix. Located in the outer third of the meniscus, fibroblast-like cells have a fusiform shape and lack a pericellular matrix. Moving through the meniscus,

intermediates between distinct cell types are found as shown in figure 2. Generally, the cells in the outer margin are more similar to fibroblasts with abundant cell processes. Moving inward the cells have less cell processes and tend to be more chondrocyte like. These cells are responsible for producing the collagen abundant extracellular matrix. This distribution of cells divides the meniscus into two sections. The fibroblast-like cells produce collagen I in the outer third, while the fibrochondrocytes produce slightly more collagen II than collagen I in the inner two thirds. The cell type also dictates the amount of GAG produced. Several studies have shown more GAG to be present in the inner two thirds than the outer portion of the meniscus which is consistent with its cellular composition [28, 29, 30].

1.4 Vasculature and Healing

In 1936, King was the first to notice the healing capability of the menisci and stated that for any healing to occur the lesion must be in contact with the blood supply [31]. Branches from the lateral medial genicular arteries form a perimeniscal capillary plexus within the synovial and capsular tissues of the knee joint, which provides the vascular supply to the margins of the menisci. During the early stages of development, the meniscus is completely vascularized. However, postnatally the inner region becomes avascular. It has been postulated that avascularity is produced by weight-bearing and knee motion. The amount of vascularization varies between the medial and lateral meniscus. The medial meniscus is typically 10-30% vascularized while the lateral meniscus has 10-25 % vascularization. Both the horn attachments of the medial and lateral meniscus have an excellent blood supply [32]. Current research suggests the inner region of the meniscus is nourished through diffusion [10].

In order for tissue to heal, it must be in contact with the blood supply. The meniscus has been divided into three regions based on vascular supply: red, red-white, and white. The red region has a considerable vascular supply, while the white zone is completely avascular. The red-white zone is the junction of the two areas. Tears in the red-red zone have great potential for healing, whereas tears in the white-white zone have virtually no healing potential. Healing potential in the red-white zone is dependent on the type of tear. Clinically when tears are in the red-red zone, tears are sutured and often heal sufficiently on their own. Unfortunately, the majority of tears occur in the inner region and require at least a partial meniscectomy [21].

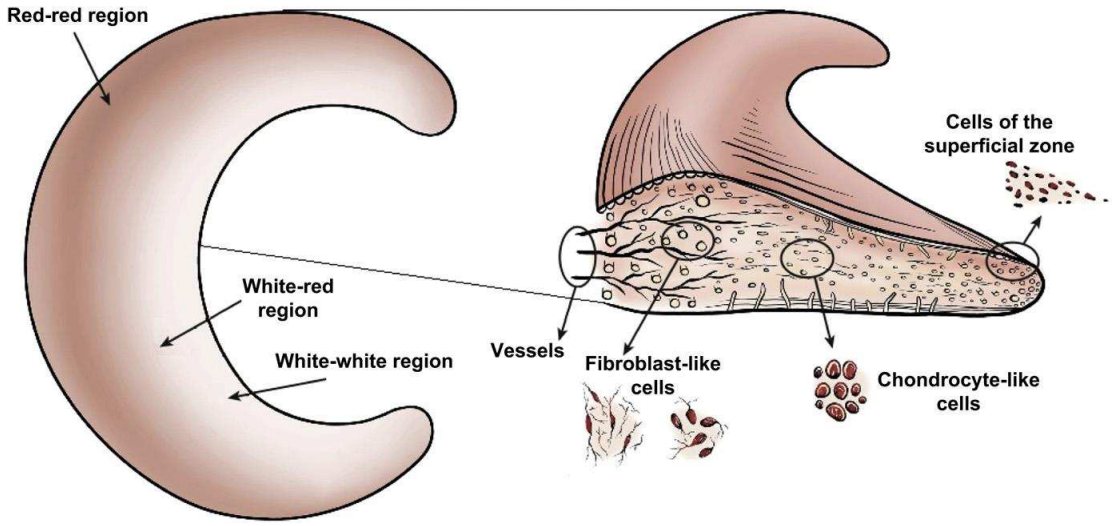

Figure 1.2. The outer third of the meniscus is vascularized with fibroblast-like cells. Moving towards the interior, the meniscus becomes avascular with chondrocyte-like cells. Image from: Makris, 2011 [8]

Osteoarthritis has been defined as "a form of chronic arthritis characterized by cartilage degradation, mildly inflammatory or noninflammatory joint fluid, joint-space narrowing, and bone sclerosis." Post traumatic osteoarthritis has been linked to traumatic overloading which may result in anterior cruciate ligament (ACL) and meniscus tears [55-57]. These studies have demonstrated degradation of proteoglycans and collagen, crucial components of the

extracellular matrix, after knee joint injury. Radin et al demonstrated that the menisci protect the articular cartilage, preventing stress concentrations and the degradation of the cartilage [34]. In 1977, Cox and Cordell used a canine model to demonstrate that damage to the meniscus caused corresponding degradation in the articular cartilage of the knee [35]. These studies illustrate the importance of a healthy meniscus to the overall health of the knee joint.

1.5 Poloxamer 188

During normal physiological events, many cells undergo various forces that may cause the plasma membrane to rupture [38]. If membrane integrity is not restored, loss of the cytoplasmic contents into the extracellular space or the rapid of influx of calcium will render the cell functionless [48]. It is therefore vital that these cells have the ability to reseal the plasma membrane [38,49]. While the exact mechanism in the repair process is still unknown, several studies have elicited certain aspects of the process [36-38]. If the disruption is small and occurs in a lipid bilayer composed only of polar lipids, the repair process will occur automatically through thermodynamics [36]. However, this is not the case for most cells. More substantial ruptures will require an active process: the formation of a membrane patch [36]. Once the plasma membrane's integrity has been compromised, a rush of extracellular calcium will signal to other vesicles within in the cell to migrate to the rupture location and fuse together creating a membrane patch [38]. Once the patch has formed, it fuses to the membrane through a process not yet fully understood. Besides restoration of the plasma membrane, the cell's cytoskeleton must also rebuild its initial architecture. The membrane patch is a temporary fix that while prolonging the cell's life, does not restore normal cell function. Several theories have been proposed on how the patch is replaced with a whole,

continuous, and functional plasma membrane [38]. One theory suggests membrane diffusion from the neighboring region as the mechanism of action. Another suggests a new plasma membrane is formed beneath the patch which is then shed. Though the exact mechanism is not well understood, it has clearly been shown this repair process is crucial to the cell's survival. Figure 1.3 illustrates this process in healthy muscle cells.

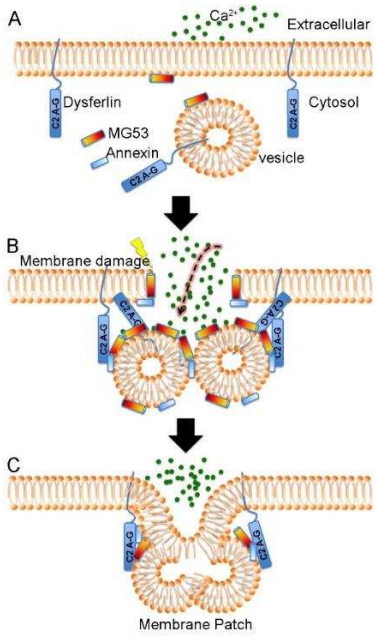

Figure 1.3. Membrane patch repair process in healthy muscle.
Calcium influx signals intracellular vesicles to membrane rupture
where the vesicles fuse together to create membrane patch.
Image from: Han, 2011 [50]

While this mechanism works for normal physiological damage, extensive injury to the cell membrane caused by trauma or disease cannot always be fixed without external intervention. This has led to an investigation into materials that may be able to aid in the plasma membrane resealing process. Mild surfactants have shown some promise in this area due to their amphiphilic properties. Poloxamer 188 (P188) is a triblock copolymer with the structure of POE-POP-POE with POE representing poly(oxyethylene) and POP poly(oxypropylene) with a molecular weight of 8400 daltons. The POP center provide a hydrophobic core while the

flanking POE chains create the hydrophilic ends giving P188 the ideal structure to insert into lipid bilayers [39].

Investigations by Maskarinec et al utilized a lipid monolayer to analyze P188 insertion into the cell membrane. They used dipalmitoylphosphatidylcholine (DPPC) and dipalmitoylphosphatidylglycerol (DPPG) molecules to form two separate monolayers. It was found that in both monolayers P188 would not insert into the monolayer until surface pressure was lowered to 22 mN/m or less. Surface pressure was then increased until P188 was "squeezed out" of the film. Pressures larger than 25 mN/m were required to eliminate the poloxamer in DPPC and larger than 28 mN/m for DPPG. The typical surface pressure for a normal bilayer is approximately 30 mN/m. As P188 does not insert into the monolayer until surface pressures are lowered to 22 mN/m, this suggests that P188 selectively inserts into damaged membrane. Because the elimination pressure is higher than the insertional pressure, this indicates that as the cell membrane heals, P188 will be released from the membrane [40]. This process can be seen in the figure below (Figure 1.4).

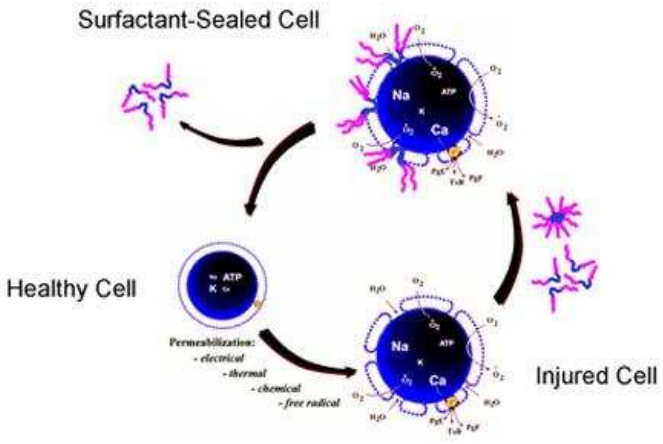

Figure 1.4. After damage to cell membrane, P188 will insert into lipid bilayer preserving cell integrity until the membrane is able to heal. Once healed, the cell will expel P188 into extracellular space.
Image from: http://www.maroonbiotech.com/research/sct.html

P188 has shown promise in sealing electropermeablized skeletal muscle membranes [41], saving neuronal cells that have undergone mechanical insult [42], and reducing cell death in knee and ankle cartilage [43,44,45]. Phillips et al examined the effect of P188 on chondral explants from bovine forelegs [39]. Explants were impacted with a load of 707 N (~25 MPa) and then incubated in media with or without P188. Cell viability was examined at two time points, 1 and 24 hours after impact, and within three zones, superficial, middle and deep. In the superficial zone, explants that were not treated with P188 had a 45% reduction in live cells at 1 hour, while after 24 hours they had 62% reduction in live cells. The middle zone of the untreated explants exhibited no differences after 1 hour, but had a 28% reduction in live cells after 24 hours. The deep zone showed no differences at either time point. Baars et al performed a similar study on bovine chondral explants and found that after 4 and 7 days post-impact, P188 reduced the percentage of cells with DNA fragmentation by 45% [43]. An *in vivo* rabbit study by Isaac et al examined the effect of P188 on knee cartilage in an unconfined impact model at 4 days and 6 weeks [51]. After 6 weeks, there was a significant higher viable cell density in the P188 treated limb compared to the untreated limb.

The effects of P188 have also been examined in human ankle cartilage [45]. An *ex vivo* study was performed using 8 mm cartilage plugs from normal human tali consisting of a 4 mm impacted core and the adjacent ring. P188 was applied for 48 hours after impact and cartilage explants were examined at 0, 2, 7 and 14 days after injury. The P188 treated explants showed significant reduced cell death in both the impacted core and the adjacent ring compared to the impacted, untreated group. There was also a significant reduction in the radial expansion of

apoptosis/necrosis into the adjacent ring for the first 7 days. This suggests that the healed cells are healthy and functioning properly.

Currently there has been only one known study that has examined the impact of P188 on the meniscus. Coatney et al performed an *in vivo* 6 week study on Giant Flemish rabbits. While no significant changes in mechanics were detected, significantly lower GAG coverage was detected in injured and untreated limbs compared to controls and injured and treated limbs [46]. Further investigation is required to determine the direct effect of P188 on the meniscus versus an *in vivo* situation where the effect could be direct or indirect.

1.6 Hypotheses and Specific Aims

Although clinically characterized by degradation of articular cartilage, osteoarthritis has been associated with meniscal injuries [4,8,21]. Traumatic overloading may result in tearing of the anterior cruciate ligament (ACL) and/or the meniscus. Tearing of the meniscus primarily results in partial meniscectomy due to its lack of healing capacity because of its avascular nature [21]. Previous studies have focused on meniscal injury due to traumatic loading both *in vivo and in vitro* [52-54]. Besides gross tissue damage, large impacts and consistent overloading due to partial meniscectomy may also have deleterious effects at the cellular level. Glycosaminoglycans (GAGs) and collagen are the primary components of meniscal extracellular matrix (ECM). Without healthy functioning cells, the ECM cannot be produced. Several studies have shown evidence of degradation of the ECM after knee joint injury [55-57]. As the ECM changes, the material properties of the meniscus may be modified, thereby changing knee joint loading and leading to joint disease such as osteoarthritis. P188 has shown promise in resealing

injured cell membranes in cartilage, neurons, and skeletal muscle [39,41-45], but its effect on meniscal tissue is unknown. Therefore, the objective of this study is to examine the effect of P188 on menisci that have undergone *in vitro* physiological and supraphysiological loads. The working hypothesis for this study is the application of P188 will mitigate the effects of overloading meniscal tissue. To test this hypothesis the following aim will be pursued.

I. To establish the efficacy of P188 in mitigating the effects of overloading meniscal tissue. Explants will undergo unconfined compression to 10% and 20% strains at a frequency of 1 Hz, to simulate walking, for 1 hour for 1 or 7 days. Cell viability and histological analysis will be utilized to investigate the effects of P188.

Hypothesis:

P188 has been shown to successfully reduce cell death after cell damage in cartilage as well as maintain GAG coverage in menisci caused by mechanical overloading. We hypothesize that in the presence of P188, the degradative effects of mechanical overloading on the meniscus will be mitigated.

REFERENCES

1. Goldblatt, John P. and John C. Richmond. *Anatomy and Biomechanics of the Knee*. Op Tech Sports Med, 2003. **11**: p. 172-186.
2. Drake, Richard L., Wayne Vogl and Adam W.M. Mitchell. *Gray's Anatomy for Students*. 2005. Philadelphia: Elsevier Inc.
3. Kohn, Dieter and B. Moreno. *Meniscus Insertion Anatomy as a Basis for Meniscus Replacement: A Morphological Cadaveric Study.* Arthroscopy. 1995, **11**: p. 96-103
4. Messner, Karola and Jizong Gao. *The menisci of the knee joint. Anatomical and functional characteristics, and a rationale for clinical treatment*. J. Anat, 1998. **193**: p. 161-178.
5. Flandry, Fred and Gabriel Hommel. *Normal Anatomy and Biomechanics of the Knee.* Sports Med Arthros Rev, 2011. **19**: p. 82-92.
6. Gupte, Chinmay M. et al. *Meniscofemoral ligaments – structural and material properties*. J Biomech, 2002 **35**: p. 1623-1629.
7. Adams, Mark E and David W. L. Hukins. The Extracellular Matrix of the Meniscus. In V. Mow, S. Arnoczky and D. Jackson (Eds.), *Knee Meniscus: Basic and Clinical Foundations*. (p. 15-28). New York: Raven Press.
8. Makris, Eleftherios A. et al. *The knee meniscus: Structure-Function, pathophysiology, current repair techniques and prospects for regeneration*. Biomaterials, 2011 **32**: p. 7411-7431.
9. Petersen, Wolf and Bernhard Tillmann. *Collagenous fibril texture of the human knee joint meniscus*. Anat Embryol, 1998. **197**: p. 317-324.
10. Arnoczky, S.P, and C.A. McDevitt. The Meniscus: Structure, Function, Repair, and Replacement. In J.A. Buckwalter, T.A. Einhorn, and S.R. Simon (Eds), *Orthopaedic Basic Science: Biology and Biomechanics of the Musculoskeletal System*. 2000. 2nd Ed. (p. 531-546). American Academy of Orthopaedic Surgeons
11. Cheung, Herman. *Distribution of Type I, II, III and V in the Pepsin Solubilized Collagens in Bovine Mensici*. Connect Tissue Res, 1987. **4**: p. 343-356.
12. Roughley, Peter et al. *The presence of a cartilage-like proteoglycan in the adult human meniscus*. Biochem J, 1981. **197**: p. 77-83.
13. McDevitt, Cahir and Richard J. Webber. *The ultrastructure and biochemistry of meniscal cartilage*. Clin Orthop Relat R. **1990**: p. 8-18.
14. Fairbank, T.J. *Knee Joint Changes After Meniscectomy*. J Bone Joint Surg Br, 1948. **30**: p. 664-670.
15. Kurosawa, Hishashi et al. *Load-Bearing Mode of the Knee Joint: Physical Behavior of the Knee Joint With or Without Menisci*. Clin Orthop Relat R. **1980**: p. 283-290.
16. Lee, Stephen et al. *Tibiofemoral Contact Mechanics After Serial Medial Meniscectomies in the Human Cadaveric Knee*. Am J Sports Med, 2006. **34**: p. 1334-1344.
17. Voloshin, Arkady S. and Josef Wosk. *Shock Absorption of Meniscectomized and Painful Knees: A Comparative In Vivo Study*. J. Biomed Eng, 1983. **5**: p. 157-161.
18. Andrews, Stephen et al. *The shocking truth about meniscus*. J. Biomech, 2011. **44**: p. 2737-2740.

19. Fithian, D. et al. *Material Properties and Structure-Function Relationships in the Menisci*. Clin Orthop Rel Res, 1990. **252**: p. 19-31.
20. Lee, S. J. et al. *Tibiofemoral Contact Mechanics After Serial Medial Meniscectomies in the Human Cadaveric Knee*. Am J Sports Med, 2006. **34**: p. 1334-1344.
21. Aagaard, H. and Verdonk, R. *Function of the normal meniscus and consequences of meniscal resection*. Scand J Med Sci Sports, 1999. **9**: 134-140.
22. Jones, S. et al. *Direct measurement of hoop strains in the intact and torn human medial meniscus*. Clin Biomech, 1996. **11**: p. 295-300.
23. Leslie, B.W. et al. *Anisotropic response of the human knee joint meniscus to unconfined compression*. Proc Instn Mech Engrs, 2000. **214**: 631-635.
24. Levy, I.M. et al. *The Effect of Medial Meniscectomy on Anterior-Posterior Motion of the Knee*. J Bone Joint Surg, 1982. **64**: p. 883-888.
25. Shoemaker, S.C., Markolf, K. L. *The Role of the Meniscus in the Anterior-Posterior Stability of the Loaded Anterior Cruciate-Deficient Knee*. J Bone J Surg, 1986. **68**: 71-79.
26. Levy, I.M. et al. *The Effect of Lateral Meniscectomy on Motion of the Knee*. J Bone Joint Surg, 1989. **71**: 401-406.
27. Musahl, V. et al. *The Effect of Medial Versus Lateral Meniscectomy on the Stability of the Anterior Cruciate Ligament – Deficient Knee.* Am J Sports Med, 2010. **38**: p. 1591-1597.
28. McDevitt, C.A. et al. *Emerging concepts of the cell biology of the meniscus.* Curr Opin Orthop, 2002. **13**: p. .345-350.
29. Sanchez-Adams, J. and Athanasiou, K.A. *The Knee Meniscus: A Complex Tissue of Diverse Cells*. Cell Mol Bioeng, 2009. **2**: p. 332-340.
30. Tanaka, T. et al. *Comparison of biochemical characteristics of cultured fibrochondrocytes isolated from the inner and outer regions of human meniscus*. Knee Surg, Sports Traumatol, Arthrosc, 1999. **7**: 75-80.
31. King, D. *The Healing of Semilunar Cartilages*. J Bone Joint Surg, 1936. **18**: p. 333-342.
32. Arnoczky, S.P and Warren, R.F. *Microvasculature of the human meniscus*. Am J Sports Med, 1982. **2**: p. 90-95.
33. McBride, I.D. and Reid, J.G. *Biomechanical Considerations of the Menisci of the Knee*. Can J Sports Sci, 1988. **4**: 175-187.
34. Radin, E. et al. *Role of the Menisci in the Distribution of Stress in the Knee*. Clin Orthop Rel Res, 1984. **185**: p. 290-294.
35. Cox, J.S. and Cordell, L.D. *The Degenerative Effects of Medial Meniscus Tears in Dogs' Knees*. Clin Orthop Rel Res. **125**: p. 236-242
36. Moloughney, J.G. and N. Weisleder. *Poloxamer 188 (P188) as a Membrane Resealing Reagent in Biomedical Applications*. Recent Pat Biotechnol, 2012: p. 200-211.
37. Abreu-Blanco, M.T. et al. *Cell wound repair in Drosophila occurs through three distinct phases of membrane and cytoskeletal remodeling*. J Cell Biol. 2011, **193**: p. 455-464.
38. Abreu-Blanco, M.T. et al. *Single cell wound repair: Dealing with life's little traumas*. BioArchitecture, 2011. **1**: p. 114-121
39. Philips, D.M. and R.C. Haut. *The use of a non-ionic surfactant (P188) to save chondrocytes from necrosis following impact loading of chondral explants.* J Orthop Res, 2004. **22**: p. 1135-1142.

40. Maskarinec, S. A. et al. *Direct Observation of Poloxamer 188 Insertion in Lipid Monolayers.* Biophys J, 2002. **82**: p. 1453-1459.
41. Lee, R.C. et al. *Surfactant-induced sealing of electropermeabilized skeletal muscle membranes in vivo*. Proc Nat Acad Sci. USA, 1992. **89**: p. 4524-4528.
42. Serbest G. et al. *The effect of Poloxamer-188 on neuronal cell recovery from mechanical injury*. J. Neurotrama, 2005. **22**: p. 119-132.
43. Baars, D.C. et al. *Treatment with the non-ionic surfactant poloxamer P188 reduces DNA fragmentation in cells from bovine chondral explants exposed to injurious unconfined compression*. Biomechan Model Mechanobiol, 2006. **5**: p. 133-139.
44. Natoli, R.M. and K.A. Athanasiou. *P188 Reduces Cell Death and IGF-I Reduces GAG Release Following Single-Impact Loading of Articular Cartilage*. J BIomech Eng, 2008. **130**: p. 041012:1-9.
45. Garrido, C.P. et al. *Anti-apoptotic treatments prevent cartilage degradation after acute trauma to human ankle cartilage*. Osteoarthr Cartilage, 2009. **17**: p. 1244-1251.
46. Coatney, G.A. et al. *Efficacy of P188 on lapine meniscus preservation following blunt trauma*. J Mech Behav Biomed Mater, 2015. **47**: p. 57-64.
47. Hoshino, A. and W.A. Wallace. *Impact-absorbing properties of the human knee*. J Bone Joint Surg Br, 1987. **69**: p. 807-811
48. Sonnemann, K.J. and W.M. Bement. *Wound Repair: Toward Understanding and Integration of Single-Cell and Multicellular Wound Responses*. Annu Rev Cell Dev Biol, 2011. **27**: p. 237-263.
49. Miyake, K. *Mechanical injury and repair of cells*. Crit Care Med, 2003. **31**: p. S496-501.
50. Han, R. *Muscle Membrane Repair and inflammatory attack in dysferlinopathy.* Skelet Muscle, 2011. **1**: 10.
51. Isaac, D.I, et al. *Acute repair of chondrocytes in the rabbit tibiofemoral joint following blunt impact using P188 surfactant and a preliminary investigation of its long-term efficacy.* J Orthop Res, 2009. **28**: p. 553-558.
52. Killian, ML. et al. *Traumatic anterior cruciate ligament tear and its implications on meniscal degradation: A preliminary novel lapine osteoarthritis model.* J Surg Res, 2010. **164**: p. 234-241.
53. Kisiday, J.D. et al. *Mechanical injury of explants from the articulating surface of the inner meniscus*. Arch Biochem Biophys, 2010. **494**: p. 138-144.
54. Hufeland, M. et al. *Response of mature meniscal tissue to a single injurious compression and interleukin-1 in vitro*. Osteoarth Cartilage, 2013. **21**: p. 209-216.
55. Lohmander, L.S. et al. *Temporal Patterns of Stomelysin-1, Tissue Inhibitor, and Proteogylcan Fragments in Human Knee Joint Fluid After Injury to the Cruicate Ligament or Meniscus*. J Ortho Res. **12**: p 21-28.
56. Lohmander, L.S. et al. *The Release of Crosslinked Peptides From Type II Collagen Into Human Synovial Fluid is Increased Soon After Joint Injury and in Osteoarthritis.* Arthritis Rheum, 2003. **48**: p. 3130-3139.
57. Struglics, A, M. Hansson, and L.S. Lohmander. *Human aggrecanase generated synovial fluid fragment levels are elevated directly after knee injuries due to proteolysis both in the inter globular and chondroitin sulfate domains*. Osteoarth Cartilage, 2011. **19**: p. 1047-1057.

58. Bursac, P. et al. *Dynamic compressive behavior of human meniscus correlates with its extra-cellular matrix composition*. Biorheology, 2009. **46**: 227-237.

CHAPTER 2: DEVELOPMENT OF BIOREACTOR GRAPHICAL USER INTERFACE

2.1 Introduction

Under normal physiological conditions, the meniscus undergoes high levels of mechanical stress, which can affect metabolic activity and disrupt meniscal cells plasma membranes [1-4]. Cellular repair is crucial to keep tissue functioning. Small ruptures in the cell membrane can be repaired through natural processes within the body [4-6]. During traumatic events, high levels of mechanical stress can create cellular membrane damage the body cannot sufficiently repair, leading researchers to explore other avenues for repair. Mimicking these physiological and traumatic loads *in vitro* using tissue explants is an effective method to observe the results of high mechanical stress on the meniscus and allow investigation of repair methods. To study these effects, *in vivo* conditions need to be simulated as closely as possible.

Depending on the nature of the study, several different approaches exist for recreating the *in vivo* environment. These devices, typically called bioreactors, can be used to recreate physiological loads on tissues or cells in the lab. Shear, compression, tension, and biaxial devices are available commercially [8]. This project's goal is to create a LabVIEW driven device to load meniscal tissue to physiological and supraphysiological loads as seen in healthy and disease states.

There are several necessary qualifications a bioreactor must meet in order to ensure successful testing. When mimicking the *in vivo* environment, great care must be taken to ensure explants remain sterile throughout the procedure. This is most readily accomplished by

ensuring that all equipment that comes into contact with the explants can be easily sterilized either by means of an autoclave or alcohol. To create the correct biochemical environment, culture media and certain additives are utilized. Constant incubation (37°C, 5% CO_2) is also required, which calls for a bioreactor made of materials that can withstand warm, humid conditions for days at a time. This was achieved using a previously validated bioreactor (Figure 2.1) [7].

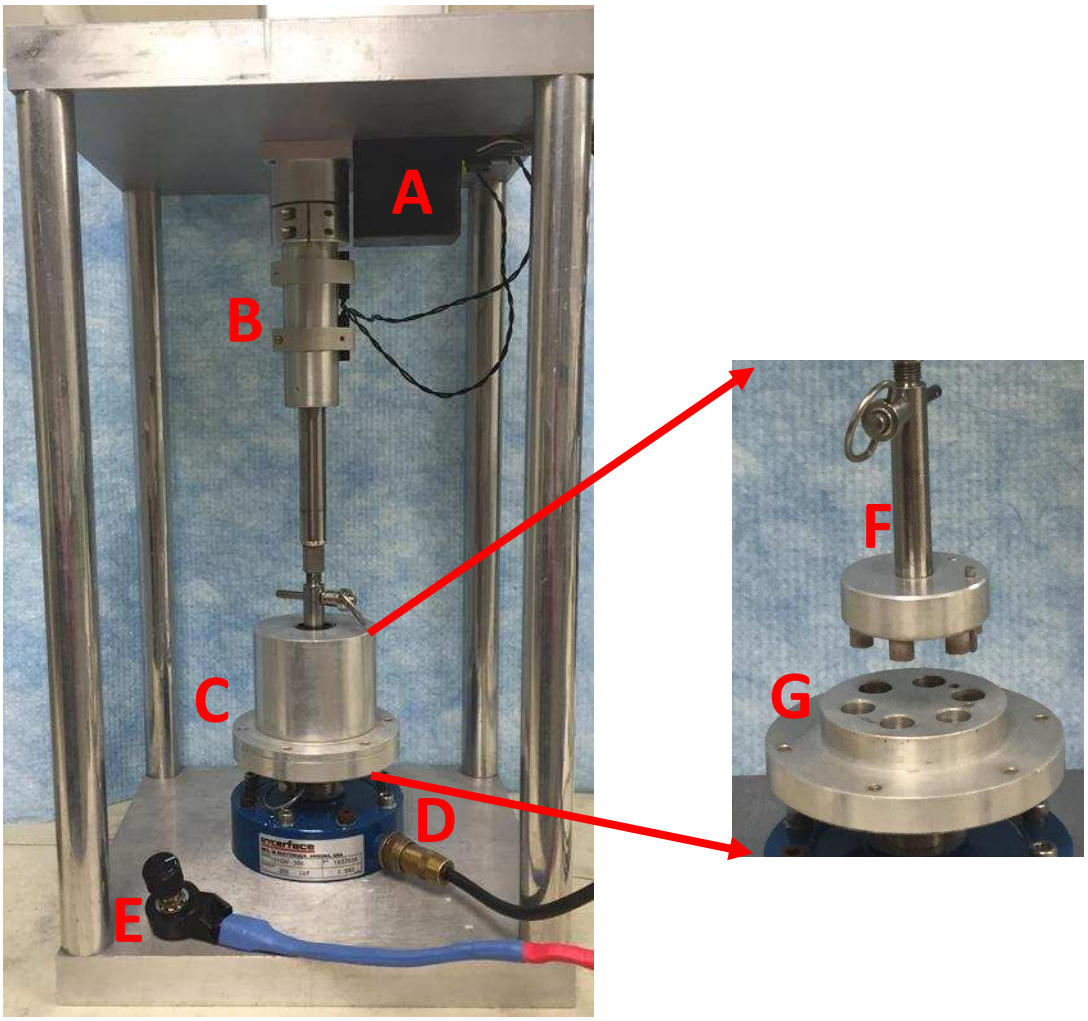

Figure 2.1. Side view of bioreactor. A) Animatics SmartMotor SM1720, B) UltraMotion Bug linear actuator, C) Enclosed well plate and plunger, D) Interface load cell, E) Honeywell optical encoder, F) plunger, G) well plate

The system consists of a belt-driven linear actuator (Ultra Motion Bug) driven by a motor (SM1720) (Ultramotion, Mattituck, NY). The actuator has a stroke length of 8.128 cm with a maximum force of 2225 N and maximum speed of 11.684 cm/sec. When built in 2003, the SmartMotor Interface(SMI), using programs written with SMI programming language, was utilized to send motor commands. However, this method of motor control has become outdated and was not user friendly. Therefore the primary purpose of this study was to update motor control by creating a user friendly graphical user interface (GUI) in LabVIEW. LabVIEW utilizes a front panel (user interface) and a block diagram (code). The user interface allows the user to change specifications for motor control without changing the code. The new program will combine manual and automatic cyclic displacements as well as control of the load cell within one easy to use graphical user interface.

2.2 Design of LabVIEW program

Several requirements must be met by the LabVIEW GUI. It is essential that the user have manual control of the bioreactor. Manual control is necessary to allow the exchange of explant groups and to properly position the plunger before starting cyclic displacement. Automatic cyclic displacement is central to the bioreactor's purpose. The number of cycles, frequency of the cycles and displacement must be easily adjustable. Data collection and monitoring of load cell output and motor position are also required. These requirements were met with the following program.

LabVIEW programming consists of a front panel and block diagram. The front panel functions as the GUI, while the block diagram contains the graphical source code of the

program. The bioreactor GUI allows the user to control manual and cyclic commands from the same simple front panel as seen in figure 2.2. There are 3 major sections on this panel: 1) Manual command, 2) Cyclic displacement command, 3) Load cell output and motor position data.

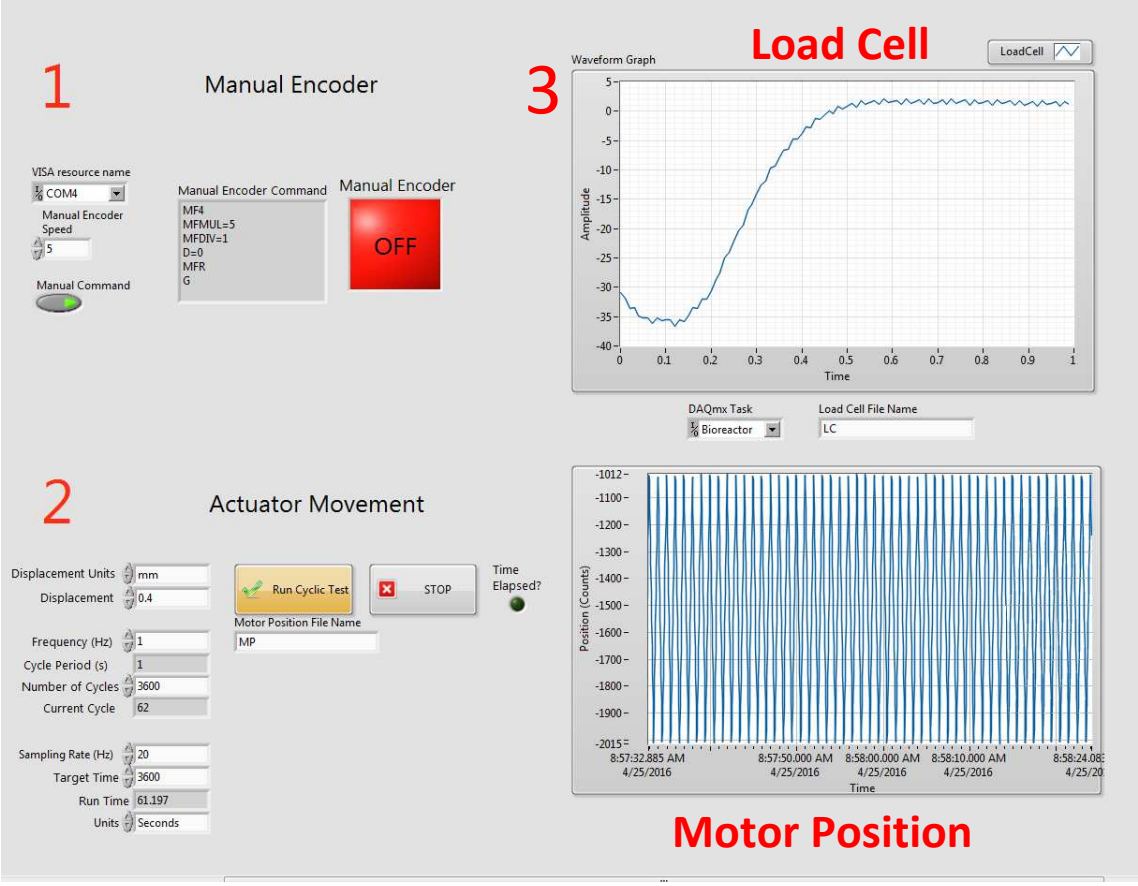

Figure 2.2. Front panel of LabVIEW program.

Manual control was achieved using an optical encoder (Honeywell, Morris Plains, NJ), which converts mechanical rotary motion into digital electrical output (Figure 2.1E). The motor has the capability to follow quadrature signals from an encoder in Mode Follow. The encoder outputs two square waves with channel A leading channel B by 90^{o} counterclockwise with continuous electrical travel. This offset allows the encoder to detect clockwise and

counterclockwise rotation. It is an incremental rotary encoder with 128 pulses per revolution and does not track absolute position. A source voltage of 5 Vdc and a supply current of 30 mA is required with an output voltage of 0.4 Vdc and 2.4 Vdc. Rotating the encoder counterclockwise raises the plunger, while rotating clockwise lowers the plunger. The manual portion of the program is controlled by section 1 of the GUI as seen in figure 2.3.

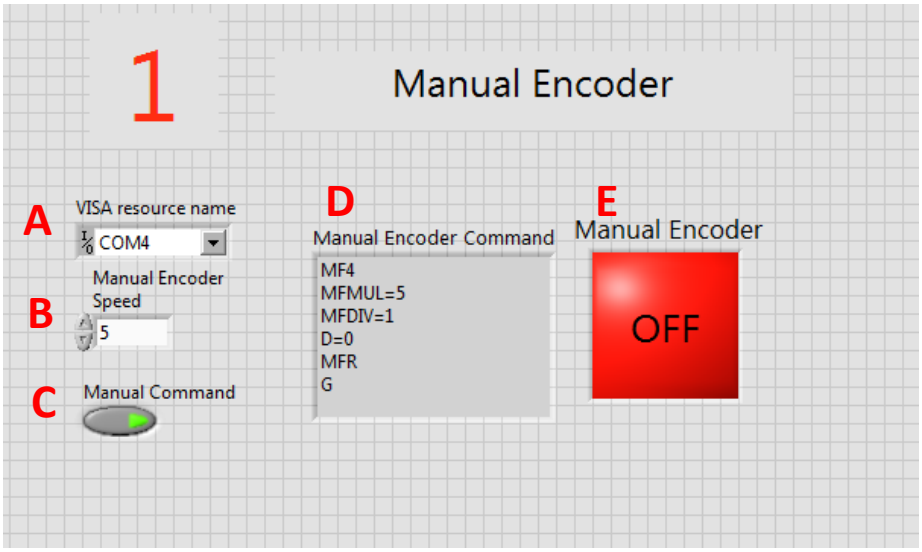

Figure 2.3. Manual command on front panel.

In order for any commands to be sent, manual or automatic, the computer must have the means to communicate with the device. VISA (Virtual Instruments Software Architecture) provides a simple avenue for communication between the motor and computer. The VISA resource name control shown in Figure 2.3A allows the user to choose the port through which the motor and computer will communicate. LabVIEW has created VISA controls specific to the method of communication between the device and computer. The SM1720 motor relies on serial communication and thus, a serial VISA control terminal was utilized on the block diagram (Figure 2.4). The serial port is straightforward to configure, allowing easy adjustments to termination characters, baud rates, data bits, etc. An advantage to using the VISA system is the

program can be operated on several platforms that support LabVIEW as VISA defines its own data types.

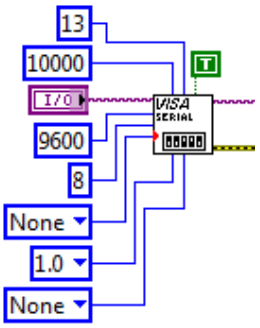

Figure 2.4. Visa serial port on block diagram.

The Manual Encoder Speed (Figure 2.3B) regulates the proportion of revolutions between the optical encoder and the linear actuator. As seen in Figure 2.3, it was set at 5 as this was found to be the optimum proportion. This was the highest it could be set without causing the belt connecting the motor and actuator to slip, disrupting the smooth linear motion of the actuator. The Manual Command play button (Figure 2.3C) turns manual control on and is active when the light is green. The Manual Encoder Command field (Figure 2.3D) allows the user to monitor the current code commanding the optical encoder. The code currently displayed shows the motor is in Mode Follow at the highest resolution (MF4) and has a 5:1 ratio of revolutions between the encoder and linear actuator. The large square Manual Encoder indicator (Figure 2.3E) turns green when the program is running and red when off.

The previously used SMI language required several calculations in order to input correct displacement and frequency for manual commands as the language communicates using motor

counts. To send a command specifying a displacement (D) of 0.5 mm, a velocity (V) of 1 mm/s with an instantaneous acceleration (A), the following would be used:

MP
A = 10000
V = 2512
D = 1256
G

This code would then have to be reentered each time the user wished to move the plunger. With this GUI, once the manual portion of the program has been activated, the user can continually move the plunger up and down as necessary without reentering code. This is due to the while loop (A) enclosing the SMI commands as seen in Figure 2.5. The commands will be continuously sent to the motor until the user authorizes the program to stop. Besides allowing serial port configuration, VISA also provides a user friendly method to read and write commands sent to the motor. VISA Write sends the data to be written to the device. VISA Read reads the data from the device such as current motor position.

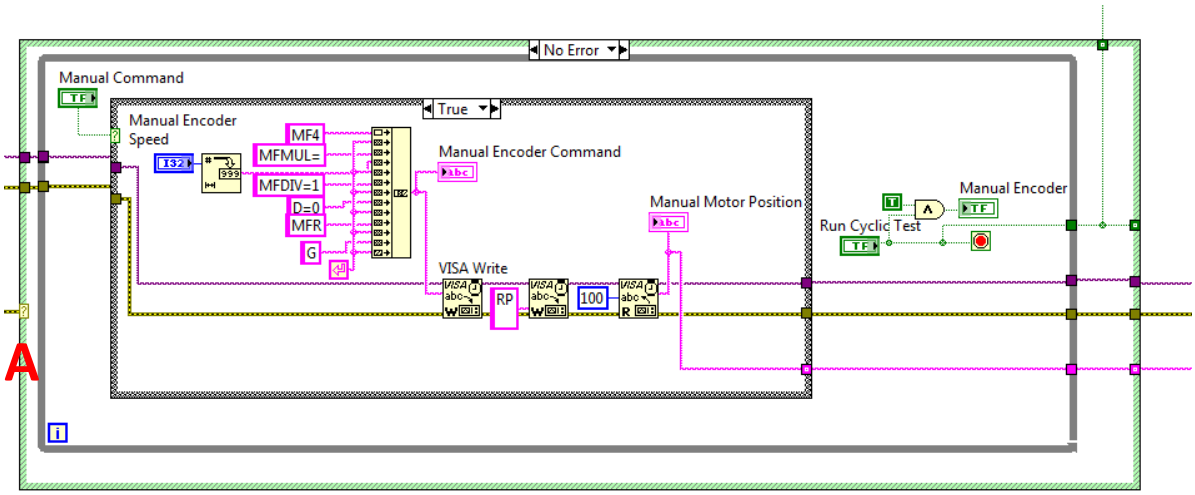

Figure 2.5. Manual command on block diagram.

Manual command is utilized to move the plunger into position above the explants. As shown in Figure 2.1, the well plate containing the explants and plunger are enclosed with a cap. The enclosed system can be easily attached or removed using quick disconnect pins. When attaching the enclosed structure, it is first connected to the load cell via one pin. The weight of the plunger (132.05 grams) serves as the preload. The manual command program is then utilized to lower the actuator to line up with the plunger and connected via another pin. Once the plunger has been attached, the cyclic displacement portion of the program may be put into effect as shown in figure 2.6.

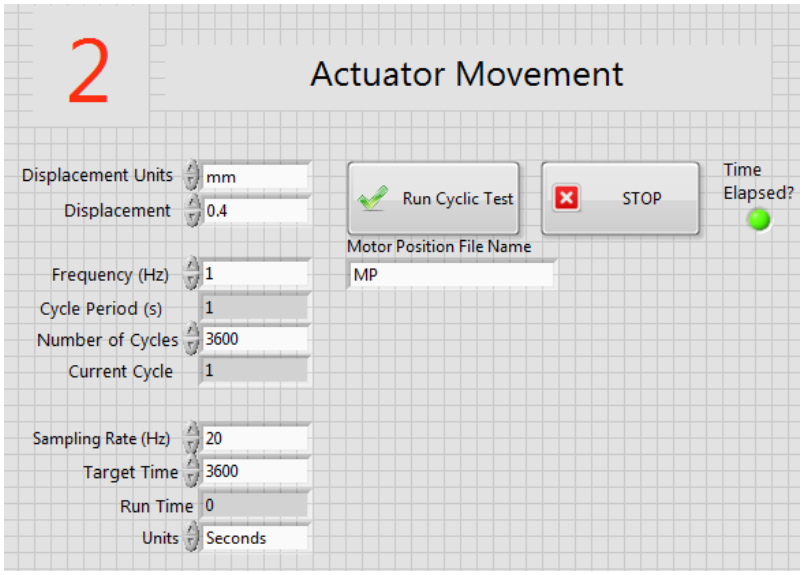

Figure 2.6. Cyclic displacement control on the front panel.

The cyclic displacement section of the program (Figure 2.6) allows the user to easily configure the bioreactor to their specifications. The white boxes are controls and indicate values that can be set by the user, while the gray boxes are indicators and are values that are reported back to the user. The previous displacement program using the SMI could only run at a frequency of 1 Hz at a specified displacement in millimeters for a specified number of cycles.

With this GUI, displacement and time units can be selected easily by the user. The commands can be sent in inches, millimeters or centimeters and seconds, minutes or hours. Frequency and number of cycles can also be easily designated. The bioreactor's current cycle is shown in the dark gray current cycle indicator box. To ensure the program is operating on the correct time frame, a separate timing loop was included in the program. A target time can be set and when the specified time has elapsed, the green indicator will light up. Below the target time entry, is the run time box which shows the real time elapsed over the course of the program. The sampling rate refers to the rate at which the motor position is recorded. 20 Hz was found to be the maximum rate at which this could occur. The limiting factor was the rate at which the motor could report position values. Motor position data is easily saved by specifying a file name in the Motor Position file name box. All data files are saved as text files.

The commands for the cyclic displacement portion are broken into two sections on the block diagram. The first section (Figure 2.7) initializes the motor (A), calculates displacement, velocity, and acceleration (B), and sends commands in the SMI language (C). Initializing the motor requires disabling displacement limits set by the manufacturer, clearing any previous errors and setting the PID (Proportional, Integral, Derivative) filter. Figure 2.7A displays the PID settings of KP = 42, KI = 28 and KD = 550 corresponding to the proportional, integral and derivative coefficients respecitively. The settings of the PID filter are used in an algorithm that delivers the necessary power required by the motor to keep the shaft on target and to reduce vibrations. The input to the PID control is position error, the desired position minus the actual position. The Proportional parameter is a spring constant and supplies the needed power to return the motor shaft to its target position. The Integral parameter is an opposing force that is

a function of time. This parameter helps the Proportional parameter bring the motor shaft back to the target position more accurately. Without the Integral parameter, the Proportional parameter would constantly oscillate around the target position. The Derivative parameter acts as a shock absorber, reducing power as a function of the rate of change of the overall PID control output and therefore dampening vibrations.

Setting the displacement, velocity and acceleration requires many calculations as the command must be sent in motor counts. In Figure 2.7C, the P refers to the absolute position of the motor. Each time the motor is shut down a new "0" position is defined. Specifically, the motor sets the "0" position as the current location of the motor when it is turned on. Therefore, to start cyclic displacement, the position of the motor must be reported when the manual control is switched off. This is accomplished utilizing VISA Read and Write as shown in Figure 2.5. From the current motor location, the required displacement can be added or subtracted to create cyclic movement of the actuator (Figure 2.7B). For example, the user inputs 2 mm as the designated displacement. 2512 motor counts is equivalent to 1 mm. The program multiplies 2 by 2512 to get the required motor counts and first subtracts then adds the specified motor counts to the absolute position to create cyclic displacement. If the user enters a positive value for the displacement, the actuator will move down initially. If a negative value is entered, the actuator will move up first. In Figure 2.7C, the A refers to acceleration. This is given an arbitrary high value to ensure instant acceleration, in this case it was set at 100,000. The V (Figure 2.7C) refers to velocity and requires the most complex computation based off the user's frequency and displacement inputs. The SmartMotor uses internally scaled counts per second as its velocity units and thus requires several multipliers to reach the desired velocity as

shown in Figure 2.7B. The motor uses a 2000 encoder count per revolution. Once the velocity has been put in terms of revolutions per second, it can be multiplied by 32,212 scaled encoder counts per second/revolution per second yielding a final velocity value that is sent to the motor.

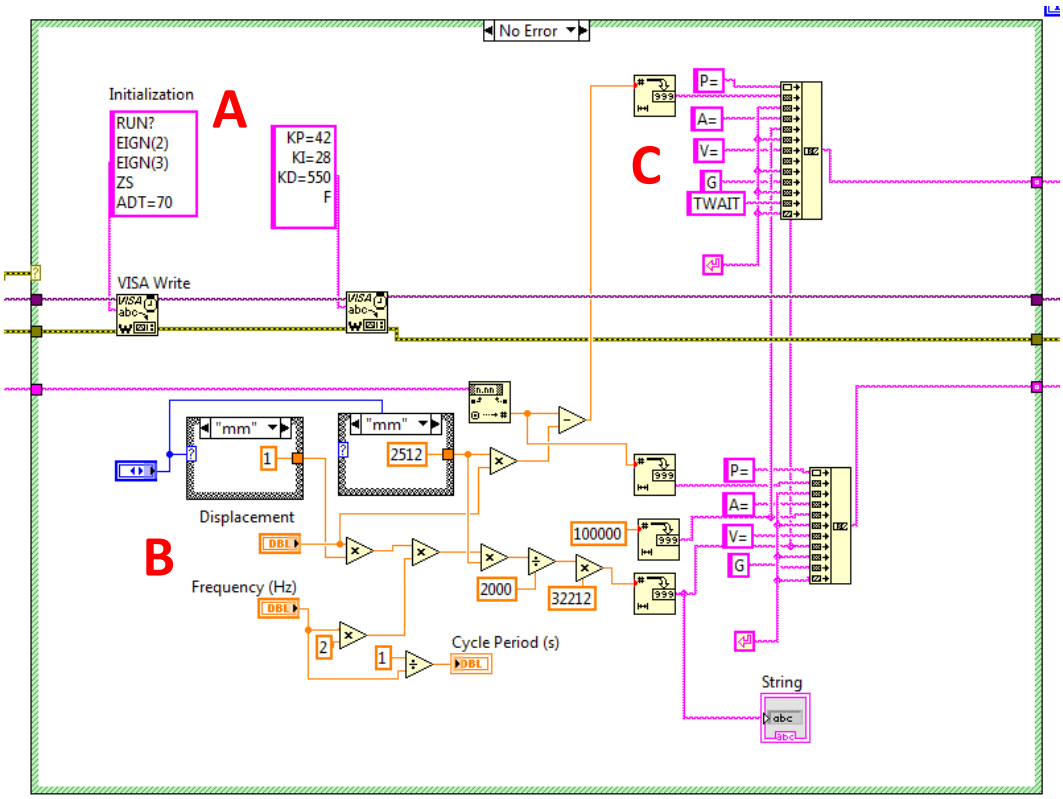

Figure 2.7. Cyclic displacement commands on block diagram.

The second section of the program (Figure 2.8) performs the specified action established by the user and initialized in the first portion of the block diagram. The external for loop (Figure 2.8A) controls the number of times the plunger compresses the explants. Each time the loop runs, the plunger moves up or down. Therefore, the loop is run twice the number of specified cycles in order to complete the requisite number of full cycles. It was also necessary to add a timing function (Figure 2.8C) to the for loop (Figure 2.8A). Without a timing

function, the loop would begin its next cycle immediately after the previous one is finished. By adding a timing function, the loop has been set to run twice during a cycle period, which is automatically calculated when the user sets a frequency. Motor position is also recorded to ensure the correct displacements are being reached. Within the for loop is a while loop (Figure 2.8B) which records motor position. The sampling rate (Figure 2.6) controls the timing for this loop. For example, when the rate is 20 Hz, then the position is recorded 20 times every second.

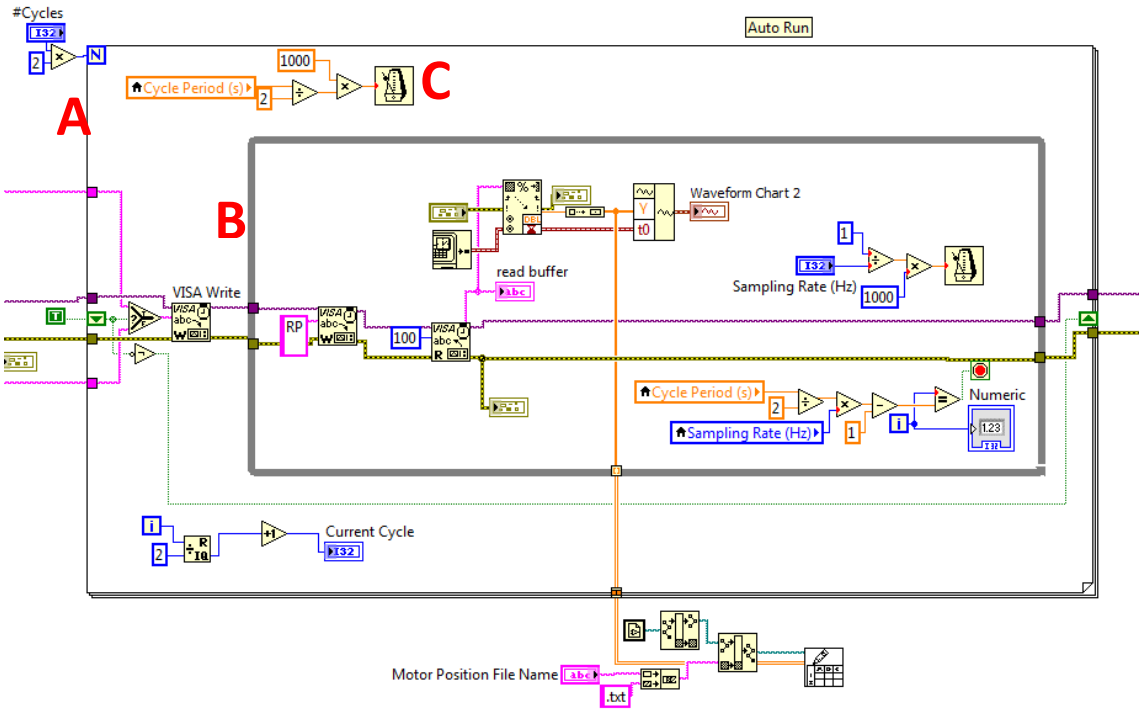

Figure 2.8. Cyclic displacement commands on block diagram (2nd section)

To ensure correct displacement while the program is running, motor position must be monitored. This was achieved with the addition of a graph monitoring motor position in the bottom right corner of the front panel (Figure 2.2). The y axis represents motor counts and the x axis is time. 2512 motor counts correspond to 1 millimeter. In Figure 2.9, the motor position

oscillates between -2015 and -1012, which corresponds to 1003 motor counts or 0.4 mm. The motor counts are negative as the plunger is lowered below the “0” position (Figure 2.9).

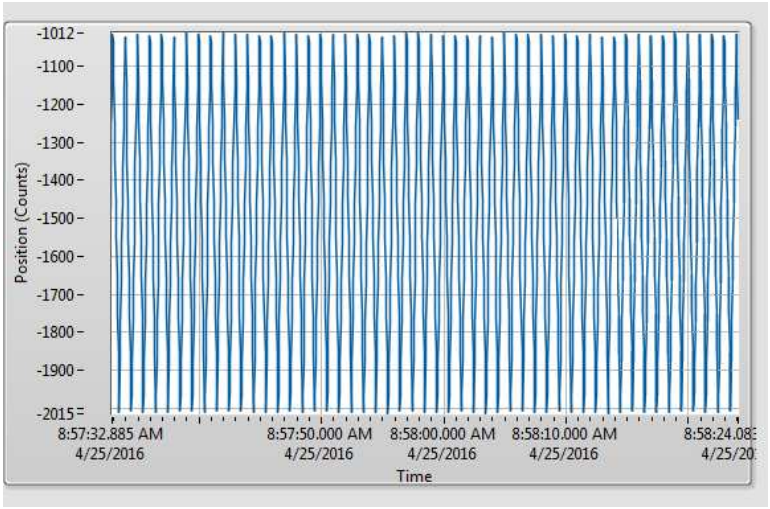

Figure 2.9. Motor position graph on front panel.

The top right section of the front panel controls the load cell. The graph shows real time data as the program is running and automatically adjusts the axes as the load changes. The y axis is load in pounds and the x axis is time (Figure 2.10). Load cell data is easily saved by specifying a file name in the Load Cell file name box. The load cell communicates with the program through a National Instruments (NI) data acquisition chassis (NI cDAQ-9174) with a NI USB-9219.

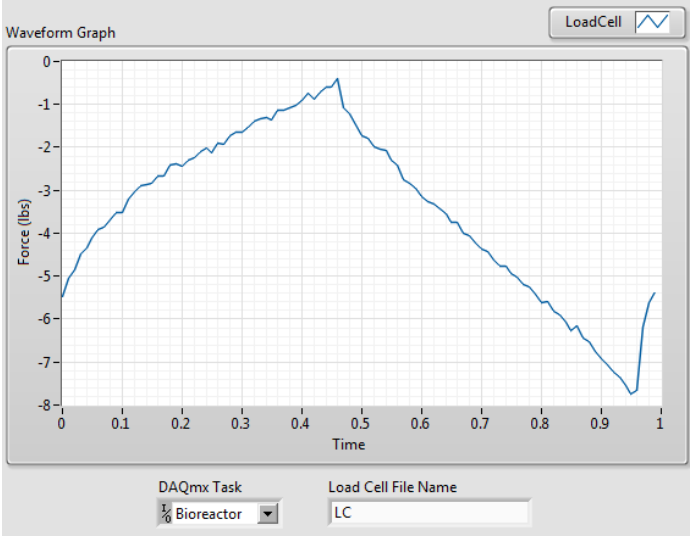

Figure 2.10. Load cell graph on front panel.

The NI USB-9219, pictured below in figure 2.11, has four channels of universal analog input and supplies a USB interface between the load cell and computer. It can support quarter, half-, and full-bridge configurations with built-in current and voltage excitation. NI-DAQmx is LabVIEW's latest data acquisition driver that provides a software interface to hardware devices. The Measurement and Automation Explorer (MAX) is utilized to access the DAQ assistant, which allows the user to create and edit virtual channels and tasks as well as input configurations for hardware devices. Tasks represent the measurement to be performed and consist of one or more virtual channels with timing and triggering properties. A virtual channel consists of a physical channel on the DAQ device and its configuration data such as the signal input range and scaling information. Global virtual channels can also be created using MAX and are defined outside of a specific task. Specifically, global virtual channels can be contained within multiple tasks. If a configuration setting is changed within the global virtual channel, the change will take effect in all tasks that include that channel. Thus multiple load cells can be easily interchanged for use with the bioreactor. By creating global virtual channels for each

load cell, they can then be selected from a drop down menu bar labeled DAQmx Task as shown in figure 2.10.

Module	Terminal	Signal Name	Signal Description
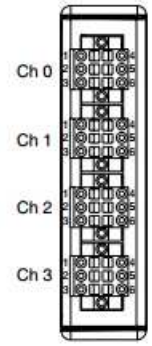	1	T+	TEDS Data
	2	T–	TEDS COM
	3	EX+/HI*	Positive excitation or input signal
	4	HI	Positive input signal
	5	EX–/LO*	Negative excitation or input signal
	6	LO	Negative input signal

Figure 2.11. NI USB-9219 signal descriptions.

The load cell code on the block diagram is setup to start when the user presses the Run Cyclic Test button (Figure 2.6). This calls the DAQmx Task, which has been defined as the load cell, to start acquiring data. The while loop runs continously for the specified number of cycles and load cell data is continously acquired. The sampling rate can be defined within the task as well. The optimum rate was 1000 Hz as it yielded the smoothest curve.

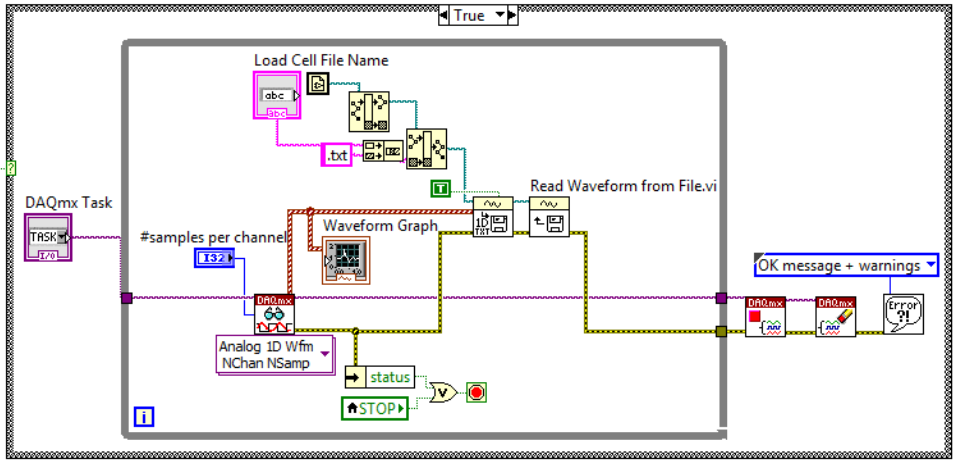

Figure 2.12. Load cell commands on block diagram.

Using DAQmx tasks also allows for easy calibration before each test. Right clicking on the DAQmx Task (Figure 2.10), pulls up a dropdown menu that gives the option to Edit DAQmx Task. This opens a new window, which allows the user to edit all load cell configuration settings as well as perform a bridge calibration (Figure 2.13). The user clicks on the Bridge Calibration tab and then Calibrate. This permits the user to zero out the weight of the well plate with explants before each compression test.

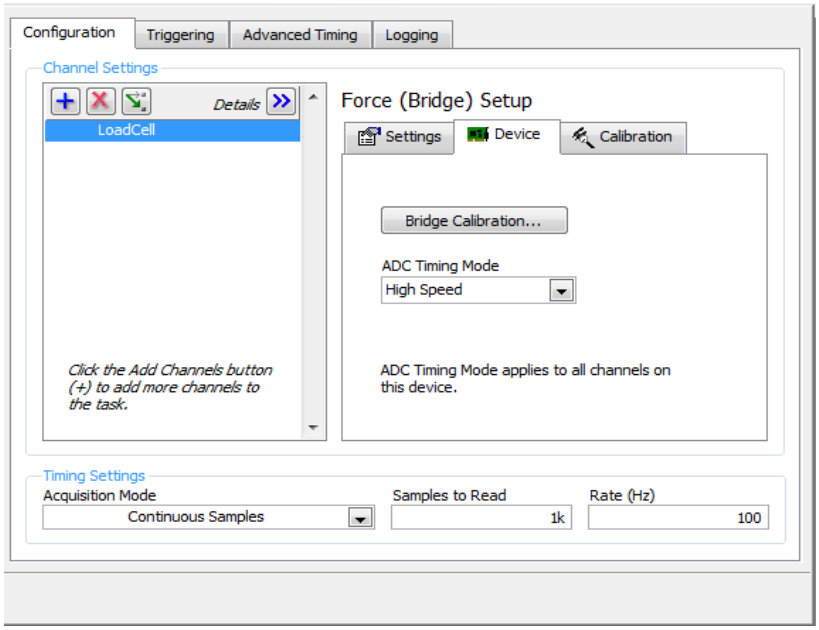

Figure 2.13. Calibration window in LabVIEW.

2.3 Validation of Bioreactor GUI

Accuracy of the bioreactor system was previously validated by McHenry et al [7]. However, to confirm accuracy of the system, it should be evaluated every other year. To ensure the frequency of the new GUI, an internal timing loop was included in the program. This loop began and ended with the cyclic displacement portion of the program. As shown in figure 2.6, the run time indicator box displayed the elapsed time. Using the number of cycles this could be back calculated to ensure precise timing.

For the purposes of this study, the bioreactor required accurate displacements between 0.1 and 1 mm. To ensure correct displacements, motor position was recorded during cyclic displacement. The program was allowed to run for 3600 cycles at various displacements. Using a Matlab program, the change in position was determined for each cycle. At 1 Hz, for a specified displacement of 0.1 mm, the average displacement was 0.105 ± 0.0004 mm. For a displacement of 1 mm, the average displacement was 1.006 ± 0.007 mm.

2.4 Discussion

The new LabVIEW GUI meets the needs of the user for cyclic displacement studies. The bioreactor maintains a sterile environment for compression tests of six meniscal explants simultaneously. Manual and automatic movement of the system has been combined into one user friendly program. Manual command allows the quick release and attachment of the enclosed well plate fixture. The cyclic displacement segment of the program offers several advantages over the previous SMI program. More parameters can be easily specified and the user is no longer limited to one frequency or set of time and displacement units. Motor position can now be constantly monitored throughout each test to ensure correct displacements are reached. The error in displacement was found to be well within an acceptable range, less than 0.1%. Load cell output can also be monitored in real time. Motor position and load cell data is saved as a text file and can be easily accessed for future analysis.

REFERENCES

1. Fink, C. et al. *The effect of dynamic mechanical compression on nitric oxide production in the meniscus*. Osteoarth Cartilage, 2001. **9**: p. 481-487.
2. Shin, S. et al. *Regulation of matrix turnover in meniscal explants: role of mechanical stress, interleukin-1, and nitric oxide*. J Appl Physiol, 2003. **95**: p. 308-313.
3. Miyake, K. and P. L. McNeil. *Mechanical Injury and Repair of Cells*. Crit Care Med, 2003. **31**: p. S496-S501.
4. Abreu-Blanco, M.T. et al. *Cell wound repair in Drosophila occurs through three distinct phases of membrane and cytoskeletal remodeling*. J Cell Biol, 2011. **193**: p. 455-464.
5. Han, R. *Muscle membrane repair and inflammatory attack in dysferlinopathy*. Skeletal Muscle, 2011. **1**: 10.
6. Abreu-Blanco, M.T. et al. *Single cell wound repair: Dealing with life's little traumas*. Bioarchitecture, 2011. **1**: 114-121.
7. McHenry, J.A. *Nitric oxide production of meniscal explants following dynamic compression*. Master's thesis, 2005. Michigan Technical University.
8. Zhao, J. et al. *Bioreactors for tissue engineering: An update.* Biochem Eng J, 2016. **109**: p. 268-281.

CHAPTER 3: EFFICACY OF P188 IN MITIGATING MENISCAL DAMAGE

3.1 Summary

Ovine meniscal explants were dynamically compressed using a custom-made bioreactor capable of displacement control testing. Knee meniscectomy has been demonstrated to increase strains and thus rupture cell membranes in the meniscus potentially leading to post-traumatic osteoarthritis. Poloxamer 188 (P188) has shown promise in mitigating tissue degradation by selective insertion into the cell membrane. Cyclic compression testing was performed on 5 mm diameter explants, 3 mm in height, at a frequency of 1 Hz for 1 hour. 10% and 20% strains were applied to the explants with and without the presence of P188 to determine the ability of P188 to prevent degradative changes as a result of high strains. These strains were chosen as 10% strain has been demonstrated to be physiological while 20% strain is considered mechanical overloading. Cell viability analysis showed a 13% reduction in cell death at 20% strain with P188. However, these effects did not continue to 7 days. No significant changes were observed in GAG coverage or mechanical properties for any group. Nitric oxide concentration was reduced by 36% at 20% strain with P188 after one day, but P188 had no effect at 7 days. These findings suggest P188 could be initially effective in mitigating tissue damage.

3.2 Introduction

The menisci are a crucial component of the knee joint. They provide smooth articulation between the rounded femoral condyles and the flat tibial plateau allowing efficient

load transfer through the joint [1-4]. The menisci consist of 72% water, while the remaining percentage is composed of extracellular matrix components (ECM) components and cells [3]. The main components of the ECM are collagen and glycosaminoglycans (GAGs). Collagen is the main fibrous component with the bulk of its fibers running circumferentially allowing the meniscus to transfer loads through the joint [5]. GAGs are part of larger molecules called proteoglycans. The proteoglycans main function is to absorb water, which gives the meniscus its compressive properties [3]. Without healthy, functioning cells, the ECM is not produced and the material properties of the meniscus change. Single, excessive compressive overloading injuries have been linked to cell membrane damage and corresponding cell death within the meniscus [6]. While the cell has a mechanism for healing small ruptures in the cell membrane, tears caused by trauma or disease cannot be fixed without external intervention [7-9]. Poloxamer 188 (P188), a synthetic surfactant, has shown a promising ability to heal cell membranes and potentially increase cell viability after injury.

Poloxamer 188 (P188) is a triblock copolymer with the structure of POE-POP-POE with POE representing poly(oxyethylene) and POP poly(oxypropylene) with a total molecular weight of 8400 daltons. The POP center provide a hydrophobic core while the flanking POE chains create the hydrophilic ends giving P188 the ideal structure to interact with lipid bilayers [10]. Previous research has demonstrated P188's ability to insert selectively into lipid monolayers based on surface pressure [11]. Several studies have also been performed *in vitro* and *in vivo* to examine the effects of P188 on skeletal muscle, neurons, and cartilage with promising results [12-17].

In cartilage, explants that have undergone an impact of 707 N and then been incubated in media in the presence of P188 for up to 7 days show a significant reduction in cell death [10,14]. Only one study has been performed investigating the effect of P188 on the meniscus. This was a six week *in vivo* study performed by Coatney et al, in which they demonstrated a significant reduction in GAG coverage loss after an injection of P188 into the injured knee in a rabbit model [17]. A gravity accelerated mass was utilized to impact the hind limb. The injured leg either received an injection of P188 or a sham injection of phosphate buffered saline (PBS) with the contralateral limb serving as a control. After six weeks, the rabbits were sacrificed and GAG coverage was analyzed. While these studies have focused on a single severe impact to the tissue, there is a shortage of data on the direct effect of P188 on the meniscus during dynamic compression to physiological and supraphysiological levels.

3.3 Methods

3.3.1 Meniscus Explants

Twenty four ovine hind limbs were obtained from the Colorado State University (CSU) Veterinary Teaching Hospital (VTH). The limbs were dissected using sterile techniques and the lateral and medial menisci were removed. A 5 mm biopsy punch was used to remove a total of 78 meniscal explants. Explants were removed from the central part of the anterior and posterior regions of the lateral and medial menisci. The explants were cut parallel to the superior surface of the meniscus.

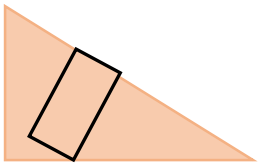

Figure 3.1 Side view of meniscus with explant cutout.

Explants were then trimmed to 3 mm in height, keeping the superior region, using an explant sizing apparatus. To allow the tissue time to equilibrate, explants were incubated for 48 hours in culture medium (89% DMEM/F12 (1:1), 10% Fetal Bovine Serum, and 1% penicillin/streptomycin) at 37^{o}C with 5% CO_2. Media was changed every 24 hours.

3.3.2 Meniscal Compression

Explants were compressed for 1 hour at 1 Hz to simulate the equivalent physiological conditions of walking for one hour. Tests were executed in the bioreactor previously mentioned. Briefly, the system is composed of a linear actuator with a motor and load cell aligned in a rigid frame in an incubator. An aluminum plate with six wells containing explants is attached to the top of the load cell. Suspended above the well plate is a plunger with six Teflon-filled Delrin compression rods controlled by the linear actuator [29]. To ensure sterility of tissue explants, the well plate and plunger are enclosed with a cap for transfer between the bioreactor and the sterile tissue hood. Before coming in contact with explants, the well plate and cap were autoclaved and the plunger sprayed thoroughly with 70% ethanol. Six explants were compressed simultaneously in unconfined compression. Meniscal explants were randomly assigned into four treatment groups (n=6): 10% strain without P188, 10% strain with P188, 20% strain without P188 and 20% strain with P188. The meniscal explants were centered in the bioreactor wells and covered with 350 uL of culture medium either with or without P188

(8 mg/ml). The plunger and cap were secured in place and then the system was transferred to the bioreactor in an incubator (37°C, 5% CO_2). The plunger was lowered until just resting on the explants and its weight was used as the preload. Samples were loaded at 1 Hz for one hour with time, position and load recorded for the duration of the test using the system software (National Instruments LabVIEW). After loading, explants were sterilely returned to the incubator with fresh medium. Samples were loaded for 1 or 7 days. Culture medium was stored after day 1 and 7 of loading at -80°C.

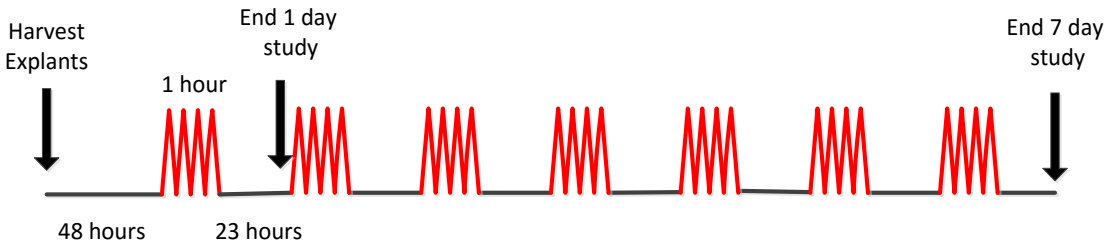

Figure 3.2 Compression cycle timeline.

Upon completion of the final loading cycle, explants were returned to the incubator for 24 hours with fresh culture medium. After post-loading culture, a center slice was taken using a scalpel (#10) for Live/Dead analysis. Half of the explant was processed for GAG analysis (Safranin O/Fast Green staining) and culture medium was stored at -80°C for NO quantification. Data collected from the load cell was analyzed for changes in material properties.

3.3.3 Live/Dead Analysis

Explant slices were stained using calcein AM and ethidium homodimer per manufacture specifications (LIVE/DEAD Viability/Cytotoxicity Kit, Molecular Probes, Eugene, OR). Explant slices were incubated in PBS containing 1 uM calcein AM and 4 uM ethidium homodimer for 25

minutes at 37°C. Following incubation, slices were then washed in PBS twice for 10 minutes at 37°C. Live and dead cell counts were determined using image analysis software (CellC, Tampere University of Technology, Tampere, Finland).

3.3.4 GAG Histology

Tissue explants were fixed in 10% formalin. After fixation, meniscal explants were immersed in a 30% sucrose solution. They were embedded in Optimal Cutting Temperature Compound (OCT) (Sakura Finetek, Torrance, CA) and flash frozen using liquid nitrogen. Explants were then cryosectioned into 6 um thick slices. Staining was performed using hematoxylin, Fast Green and Safranin O, which stain cell nuclei black, cytoplasm blue, and GAG red respectively (Appendix 5.2.6). Slices were imaged using a Leitz Laborlux S microscope (Leitz, Oberkochen, Germany) and Olympus DP25 camera (Olympus, Center Valley, PA).

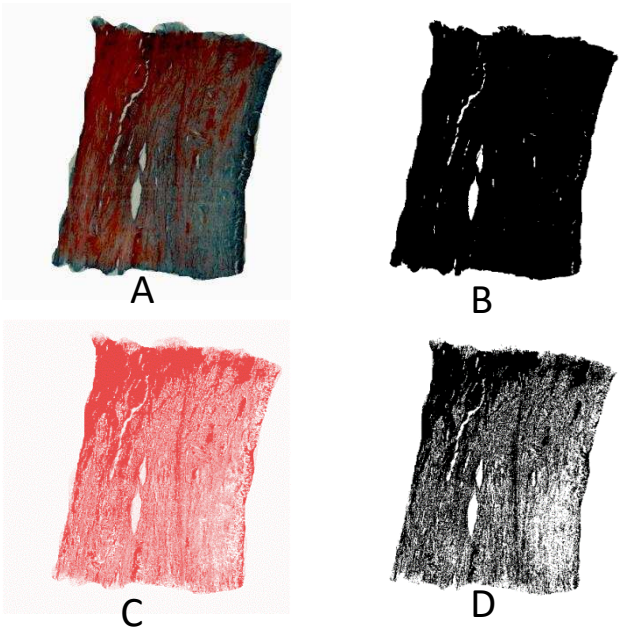

Figure 3.3 A) Full color image of meniscus B) Analyze particles tool for whole menisci C) Color deconvolution tool for area stained with GAG (red) D) Analyze particles area for area stained with GAG

GAG coverage was analyzed using Image J (NIH, Bethesda, MD) with FIJI package. Images were converted to 8 bit images. The Analyze Particles tool was utilized to determine total area of the image. The area stained red is associated with GAG coverage and was separated from the image using the Color Deconvolution tool. The image could then undergo thresholding and analyze particles to determine GAG coverage. These areas were used to calculate a GAG coverage percentage (Figure 3.3).

3.3.5 Nitric Oxide Quantification

Total nitric oxide was quantified from conditioned media as per manufacturer's instructions (Cayman Chemical, Ann Arbor, MI) (Appendix 5.2.7). Briefly, nitric oxide exists in two stable forms, nitrate and nitrite. The assay converts all nitrate to nitrite using the Griess reaction, which produces a colored azo dye. Absorption is read at 540 nm using a spectrophotometer. Using known concentrations of nitrite, a standard curve (Appendix 5.3.3) is generated and utilized to convert absorption values to concentration.

3.3.6 Material Properties Analysis

Matlab was utilized to take the absolute value of the force vs time curve. For each compression test, the local peaks were found. A second order power curve, y = a*x^b+c, was fit to the data. The local peak values were averaged for each group for each time point, resulting in one curve fit per group per time point.

3.3.7 Statistical Analysis

One-way analysis of variance (ANOVA) with a post hoc Tukey test using Minitab software (Minitab17, State College, PA) was performed on cell viability, GAG coverage, and NO assay

data to assess differences between strain levels and P188 treated and non-treated groups. Regression analysis was utilized to determine changes in material properties of menisci. R-squared values were used to determine fit of regression. $P < 0.05$ was considered significant for all tests

3.4 Results

3.4.1 Live/Dead

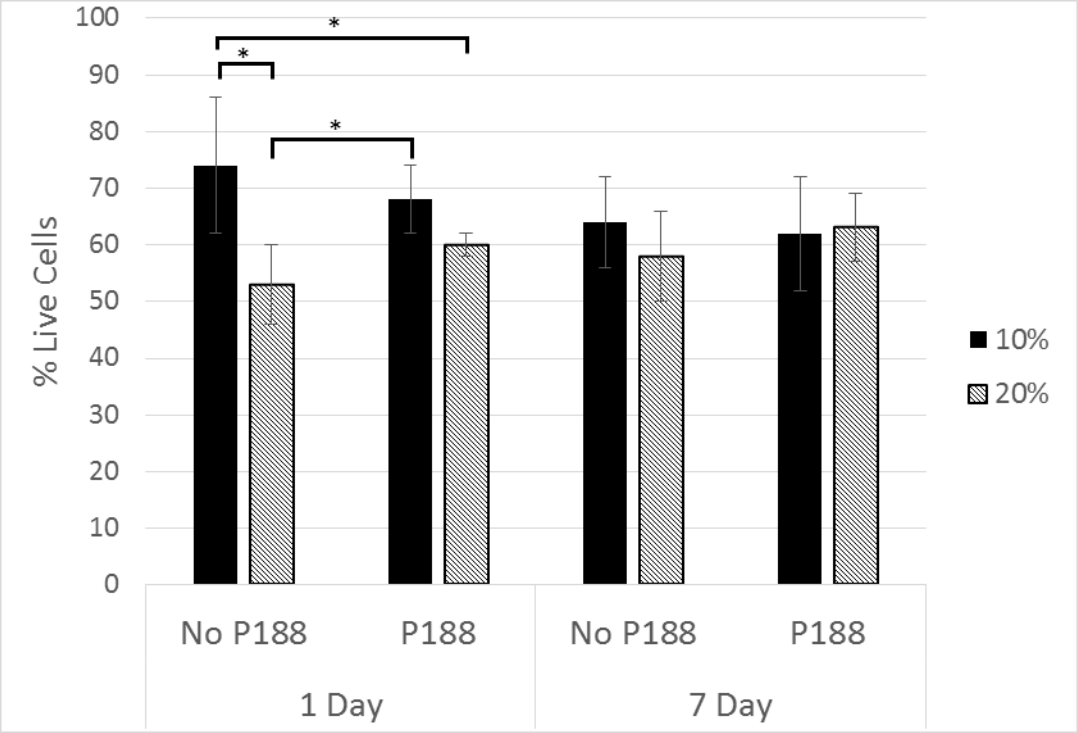

Figure 3.4. Results from Live/Dead assay for 1 and 7 day studies. * denotes significance $p<0.05$

Significant differences were found after 1 day of compression ($p<0.001$) (Figure 3.4). Without P188, the 10% strain group had an increased percentage (21%) live cells compared to group undergoing 20% strain. Significant differences were also shown between 20% strain without P188 and 10% strain with P188 as well as between 10% without P188 and 20% with

P188. After seven days of compression, there were no significant differences between groups with or without P188 or between 10% and 20% strains.

3.4.2 GAG

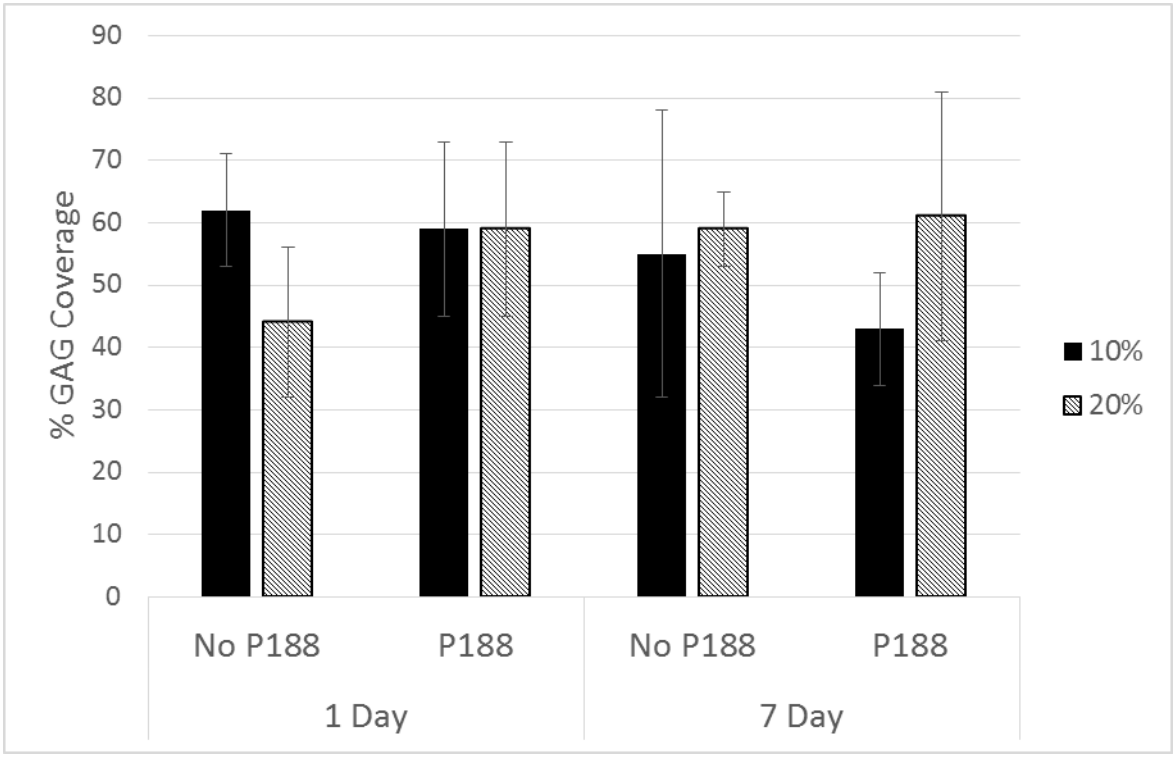

Figure 3.5. Comparison of GAG coverage for 1 and 7 days. ANOVA revealed no significant differences between strain groups, with or without P188.

No significant differences were found in percent GAG coverage after one or seven days (Figure 3.5), between groups with or without P188, or between strain groups. However, while not significant, there was a decrease in GAG coverage for samples compressed to 20% without P188 compared to only 10% compression.

3.4.3 NO Assay

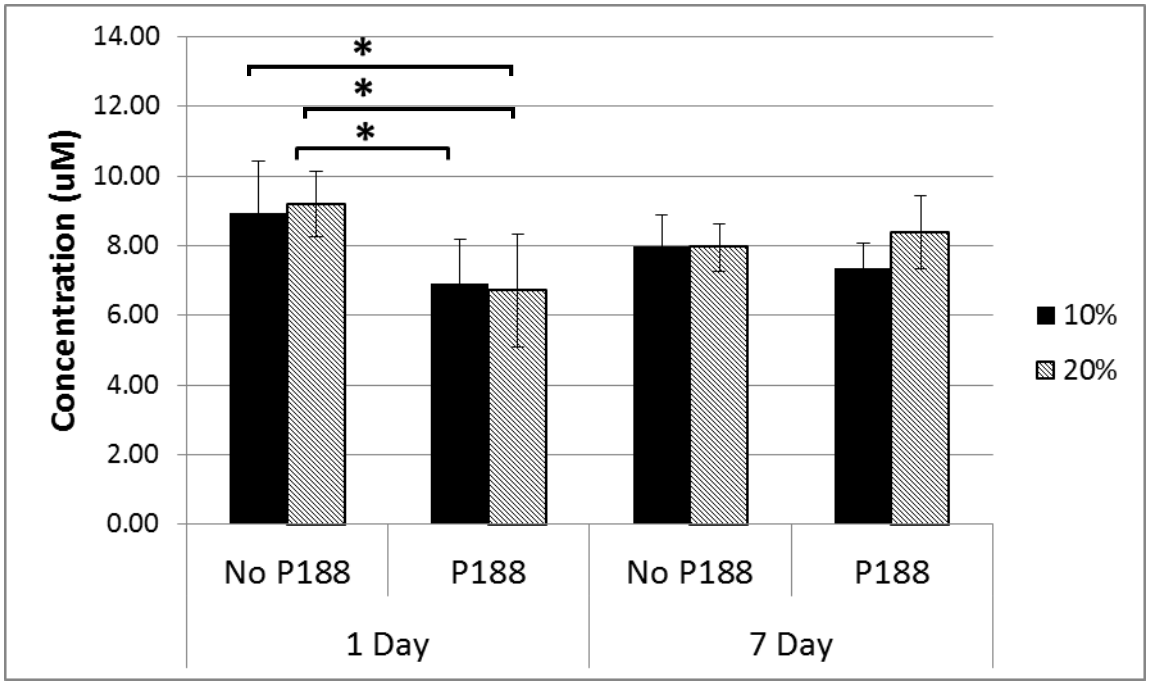

Figure 3.6. Comparison of nitric oxide concentration for 1 and 7 days. * denotes significance $p<0.05$

After 1 day, general trends showed smaller NO concentrations in the groups treated with P188 compared to the non-treated groups (Figure 3.6). There were no significant differences between 10% strain groups with or without P188. NO concentration was also found to be significantly lower in the 20% strain P188 treated group compared to the 10% and 20% groups without P188 ($p<0.006$). The 10% P188 treated group was significantly lower than the 20% non-treated group ($p<0.006$). No significant differences were found after 7 days between strain groups or between groups with or without P188.

3.4.4 Mechanical Data

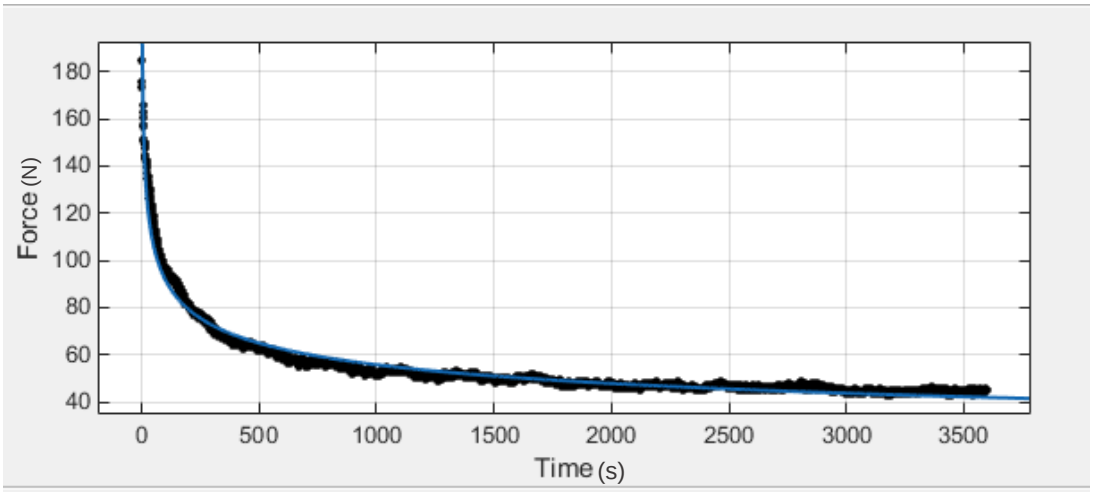

Figure 3.7. Representative data for second order power curve fit.

Using force peaks isolated from the cyclic displacement graphs versus time, a second order power curve, y = a*x^b+c, was fit to the data. In the first 500 cycles a rapid drop in load occurred with little change for the remaining 3000. Figure 3.7 shows an example of the 20% strain group without P188 from the seventh day of a seven day study.

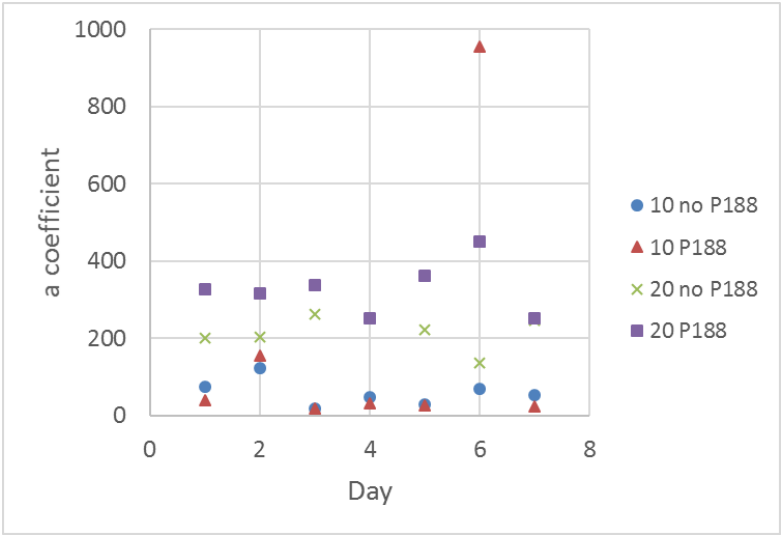

Figure 3.8. “a” coefficient over 7 days for both strain groups, with and without P188. Linear regression analysis revealed no significant differences over 7 days for strain groups or with/without P188.

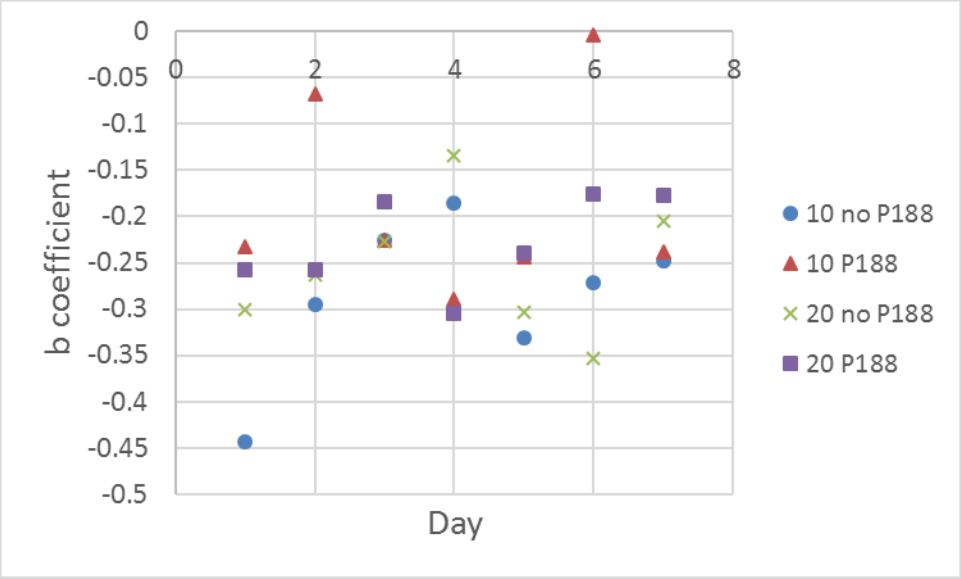

Figure 3.9. "b" coefficient over 7 days for both strain groups, with and without P188. Linear regression analysis revealed no significant differences over 7 days for strain groups or with/without P188.

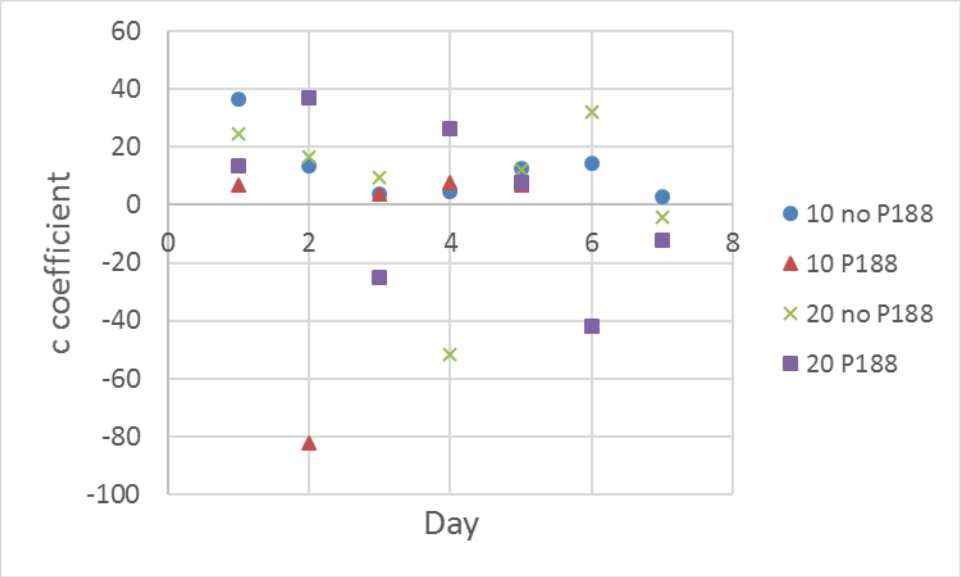

Figure 3.10. "c" coefficient over 7 days for both strain groups, with and without P188. Linear regression analysis revealed no significant differences over 7 days for strain groups or with/without P188.

The coefficients of these curves (a,b,c) (Appendix 5.3.4) were compared over time using linear regression within groups to examine changes in material properties (Figure 3.8-10): a relates to stiffness, b to time-dependence and c is a scaling factor. No significant differences were found between strain groups or P188 treated and non-treated groups.

3.5 Discussion

Previous research has shown the intact meniscus undergoes 10% strain physiologically, while removal of 30% of the meniscus caused strains to almost double to 20% [19]. Hence these two strains were chosen for dynamic compression testing as physiological and supraphysiological. It was expected that a strain of 20% would cause significant cell death in comparison to 10% strain. Cell viability assays showed promise in "saving" cells that had been overloaded at the one day mark. There was no significant difference in cell viability between 10% strains groups treated or non-treated, indicating that P188 does not have adverse effects at physiological strains. As expected, significant differences did occur between 10% and 20% strain in the non-treated group. The 10% strain level had a higher percentage of live cells (21%) compared to 20% strain. With the application of P188, this difference was decreased to 8%. Although the percentage of healthy cells did not recover to initial levels at the 10% strain no P188 group, there was a significant reduction in cell death. Phillips and Haut demonstrated increases in cell viability as high as 49% in chondrocytes with the application of P188 over a 24 hour period [10]. Baars et al showed a 45% reduction in DNA fragmentation up to 7 days post-impact in the presence of P188 [14]. However, both studies performed a single injurious impact to the chondrocyte versus consistent dynamic strains. While P188 may have beneficial effects after an initial traumatic impact, its efficacy may be reduced with consistent overloading. Dynamic loading may also contribute to "washing out" dead cells over the course of seven days. These cells may be removed from the tissue and released into the cell media. Future studies should assay the media for live and dead cells to gain a full representation of cell viability within the meniscus. Fithian et al also demonstrated that bovine meniscal tissue has

one-sixth the permeability of articular cartilage [18]. This difference in permeability may account for the difference in cell viability in cartilage vs meniscus tissue. Fluorescent labeling may be a viable option to track diffusion of P188 into the meniscus and optimize P188 concentration. Cartilage consists of a single cell type, chondrocytes, whereas menisci have fibroblast- and chondrocyte-like cells. Fibroblast-like cells are found at the outer third of the meniscus, but the inner two-thirds consist of chondrocyte-like cells. P188 may affect each cell type differently and in turn affect each zone of the meniscus in distinctive ways. Further investigation is necessary to elucidate the effect of P188 on each cell type.

GAG is an essential part of proper biomechanical function as it chemical properties retain water, which endows the meniscus with its compressive abilities [20,21]. The loss of GAG is associated with reductions in the coefficient of viscosity and modulus of relaxation [21]. Over the seven day study, there were no significant changes in GAG coverage between strain levels or P188 treated or non-treated groups. As there was no change in GAG coverage, it was expected there were be no change in mechanical properties. Mechanical data from this study indicated no change in mechanical properties supporting this conclusion. In the only known study investigating the effect of P188 on the meniscus, Coatney et al demonstrated in an *in vivo* study over 6 weeks, that P188 was able to retain GAG coverage compared to the non-treated groups [17]. However, despite this change in GAG coverage, changes in mechanical properties were not observed. This largely may be due to the small sample size. Little to no research has been done on the time frame over which material properties of the meniscus change. Further investigation is necessary in order to correlate changes in GAG coverage with mechanical properties, as remodeling of meniscal tissue is poorly understood.

Despite not observing altered mechanical properties, Coatney et al observed significant changes in GAG coverage over 6 weeks in impacted, non-treated limbs *in vivo*. Seven days may not be a substantial amount of time to observe changes in GAG coverage in meniscal explants. By extending the study to 14 or 21 days, changes in GAG coverage may be observed. However, this extended period of time *in vitro* may be difficult to attain in culture with sterility. There is a great deal of conflicting literature on how GAG is affected by mechanical overloading. Two methods of assessing GAG levels are commonly used. The first is as described in this study, using histological means to assess GAG coverage of a cross-section of the tissue. The second method is assaying GAG concentrations in conditioned media. However, no means of comparing these two assays has been developed. A study by Hufeland et al demonstrated a single compression with a strain of 50% was necessary to increase GAG release to the media [22]. Killian et al showed upregulated GAG concentrations in the media occurred at 20% dynamic strain [23]. GAG concentrations may increase in the media immediately after compressive cycles, but this change may take multiple weeks for a visual change to occur in GAG coverage within the tissue. Further investigation into this relationship is required.

High concentrations of nitric oxide have been found in osteoarthritic synovial fluid and is believed to regulate catabolic activity in meniscus and cartilage [24, 25]. High levels of NO cause tissue degradation, by reducing production of collagen II, and apoptotic cell death [26,27,28]. McHenry investigated the relationship between NO concentration and dynamic compression of meniscal explants in load and displacement controlled experiments and found NO concentration was upregulated at 20% strain [29]. Fink et al and Shin et al also showed an upregulation of NO in dynamic compression [30, 31]. However, they compressed meniscal

explants consistently for 24 hours, which is not physiologically realistic. In this study, increased levels of strain did not affect the NO concentration in the untreated group. The explants were only compressed for one hour and that may not have been sufficient to see strain dependent changes in NO concentration. However, both 10% and 20% strain groups had decreased NO concentration with the application of P188. There was 36% reduction in NO concentration between 20% treated and untreated groups. This indicates the P188 may be interfering with the NO signaling cascade, which could slow tissue degradation.

To the best of our knowledge, this is the first study to directly examine the effects of P188 on the dynamic compression of meniscal explants. The bioreactor setup mimics an hour of walking per day in an attempt to understand how P188 interacts with physiological and supraphysiological loaded meniscal tissue. While P188 shows promising results within the first 24 hours, this study had several limitations. Small samples sizes limited determination of mechanical properties. Due to the setup of the bioreactor only two independent mechanical data sets were available per group. The concentration of P188 had been earlier optimized for cartilage explants [10]. Due to differences in permeability between cartilage and meniscus an optimization of P188 concentration may be necessary for the meniscus. While there were no visible changes in viscosity, future investigations should examine the effect of P188 on media viscosity to ensure there is no interference in loading with the bioreactor or in meniscal tissue uptake. Longer time periods should also be examined, particularly to investigate changes in GAG coverage. P188 shows promising results in the first 24 hours and appears to “save” cells. It is currently unknown, whether these “saved” cells will still function as normal, healthy cells. Although they appear to be alive according to Live/Dead assays, the damage due to overloading

may cause the cells to form an abnormal matrix leading to changes in material properties. The best course of action could be to let the cells go through the natural process of cell death. Further investigation is needed to ascertain the effect of these "saved" cells on the surrounding matrix. Polymerase chain reaction (PCR) could be utilized to examine various biomarkers that indicate cell health. Pharmaceutical intervention is an encouraging avenue to consider to mitigate molecular damage after mechanical trauma to meniscal tissue. Further investigation of P188 may provide a method to slow tissue degradation and prevent the development of osteoarthritis.

REFERENCES

1. Messner, Karola and Jizong Gao. *The menisci of the knee joint. Anatomical and functional characteristics, and a rationale for clinical treatment*. J. Anat, 1998. **193**: p. 161-178.
2. Fox, A.J.S. et al. *The Human Meniscus: A Review of Anatomy, Function, Injury, and Advances in Treatment*. Clin Anat, 2015. **28**: p. 269-287.
3. Makris, Eleftherios A. et al. *The knee meniscus: Structure-Function, pathophysiology, current repair techniques and prospects for regeneration*. Biomaterials, 2011 **32**: p. 7411-7431.
4. Kurosawa, Hishashi et al. *Load-Bearing Mode of the Knee Joint: Physical Behavior of the Knee Joint With or Without Menisci*. Clin Orthop Relat R. **1980**: p. 283-290.
5. Aagaard, H. and Verdonk, R. *Function of the normal meniscus and consequences of meniscal resection*. Scand J Med Sci Sports, 1999. **9**: p. 134-140.
6. Hufeland, M. et al. *Response of mature meniscal tissue to a single injurious compression and interleukin-1 in vitro.* Osteoarth Cartilage, 2013. **21**: p. 209-216
7. Moloughney, J.G. and N. Weisleder. *Poloxamer 188 (P188) as a Membrane Resealing Reagent in Biomedical Applications*. Recent Pat Biotechnol, 2012: p. 200-211.
8. Abreu-Blanco, M.T. et al. *Cell wound repair in Drosophila occurs through three distinct phases of membrane and cytoskeletal remodeling*. J Cell Biol. 2011, **193**: p. 455-464.
9. Abreu-Blanco, M.T. et al. *Single cell wound repair: Dealing with life's little traumas*. BioArchitecture, 2011. **1**: p. 114-121
10. Philips, D.M. and R.C. Haut. *The use of a non-ionic surfactant (P188) to save chondrocytes from necrosis following impact loading of chondral explants.* J Orthop Res, 2004. **22**: p. 1135-1142.
11. Maskarinec, S. A. et al. *Direct Observation of Poloxamer 188 Insertion in Lipid Monolayers.* Biophys J, 2002. **82**: p. 1453-1459.
12. Lee, R.C. et al. *Surfactant-induced sealing of electropermeabilized skeletal muscle membranes in vivo*. Proc Nat Acad Sci. USA, 1992. **89**: p. 4524-4528.
13. Serbest G. et al. *The effect of Poloxamer-188 on neuronal cell recovery from mechanical injury*. J. Neurotrama, 2005. **22**: p. 119-132.
14. Baars, D.C. et al. *Treatment with the non-ionic surfactant poloxamer P188 reduces DNA fragmentation in cells from bovine chondral explants exposed to injurious unconfined compression*. Biomechan Model Mechanobiol, 2006. **5**: p. 133-139.
15. Natoli, R.M. and K.A. Athanasiou. *P188 Reduces Cell Death and IGF-I Reduces GAG Release Following Single-Impact Loading of Articular Cartilage*. J BIomech Eng, 2008. **130**: p. 041012:1-9.
16. Garrido, C.P. et al. *Anti-apoptotic treatments prevent cartilage degradation after acute trauma to human ankle cartilage*. Osteoarthr Cartilage, 2009. **17**: p. 1244-1251.
17. Coatney, G.A. et al. *Efficacy of P188 on lapine meniscus preservation following blunt trauma*. J Mech Behav Biomed Mater, 2015. **47**: p. 57-64.
18. Fithian, D. et al. *Material Properties and Structure-Function Relationships in the Menisci*. Clin Orthop Rel Res, 1990. **252**: p. 19-31.

19. Zielinska, B. and T.L. Haut Donahue. *3D Finite Element Model of Meniscectomy: Changes in Joint Contact Behavoir*. J Biomech Eng, 2006. **128**: p. 115-123
20. Bursac, P. et al. *Dynamic compressive behavior of human meniscus correlates with its extra-cellular matrix composition*. Biorheology, 2009. **46**: 227-237.
21. Sanchez-Adams, J et al. *Regional variation in the mechanical role of knee meniscus glycosaminoglycans*. J Applied Physiol, 2011. **111**: p. 1590-1596.
22. Hufeland, M. et al. *Response of mature meniscal tissue to a single injurious compression and interleukin-1 in vitro*. Ostearth Cartilage, 2013. **21**: p. 209-216.
23. Killian, M.L. et al. *In vitro inhibition of compression-induced catabolic gene expression in meniscal explants following treatment with IL-1 receptor antagonist*. J Orthop Sci, 2011. **16**: p. 212-220.
24. Hashimoto, S. et al. *Nitric Oxide and Apoptosis in Cells of the Meniscus During Experimental Osteoarthritis*. Arthritis Rheum, 1999. **10**: 2123-2131.
25. Kobayashi, K. et al. *Chondrocyte apoptosis and regional differential expression of nitric oxide in the medial meniscus following partial meniscectomy*. J Orthop Res, 2001. **19**: 802-808.
26. Cao, M. et al. *Nitric oxide inhibits the synthesis of type-II collagen without altering Col2A1 mRNA abundance: prolyl hydroxylase as a possible target*. Biochem J, 1997. **324**: 305-310.
27. Cao, M. et al. *Generation of Nitric Oxide by Lapine Meniscal Cells and Its Effect on Matrix Metabolism: Stimulation of Collagen Production by Arginine*. J Orthop Res, 1998. **16**: 104-111.
28. Gupta, T. et al. *IL-1 and iNOS gene expression and NO synthesis in the superioe region of meniscal explants are dependent on the magnitude of compressive strains*. Osteoarth Cartilage, 2008. **16**: 1213-1219.
29. McHenry, J.A. *Nitric oxide production of meniscal explants following dynamic compression*. Master's thesis, 2005. Michigan Technical University.
30. Fink, C. et al. *The effect of dynamic mechanical compression on nitric oxide production in the meniscus*. Osteoarth Cartilage, 2001. **9**: p. 481-487.
31. Shin, S. et al. *Regulation of matrix turnover in meniscal explants: role of mechanical stress, interleukin-1, and nitric oxide*. J Appl Physiol, 2003. **95**: p. 308-313.

CHAPTER 4: CONCLUSION

To investigate the effects of P188 on the meniscus, the goals of this project were to: 1) create a user friendly graphical user interface (GUI) for a custom bioreactor capable of displacement control for precise loading of meniscal explants to physiological and supraphysiological strains; 2) determine the efficacy of P188 in mitigating meniscal tissue damage through cell viability, mechanical data and histological analysis.

Briefly, the bioreactor consists of a linear actuator with a motor and load cell aligned in a rigid frame in an incubator. An aluminum plate with six wells containing explants is attached to the top of the load cell. Suspended above the well plate is a plunger with six Teflon-filled Delrin compression rods controlled by the linear actuator. The bioreactor maintains a sterile environment for compression tests of meniscal explants. To meet the requirements of the user, the bioreactor must be capable of manual control, displacement control, real time monitoring of motor position and load cell data, and interchangeable load cells that are easily calibrated. Manual and automatic movement of the system has been combined into one user friendly program. Manual command was achieved with the use of a rotary optical encoder, which allows the quick release and attachment of the enclosed well plate fixture. The cyclic displacement segment of the program offers several advantages over the previous SMI program. More parameters can be easily specified and the user is no longer limited to one frequency or set of time and displacement units. The bioreactor can be run for one hour or continuously over multiple days. Motor position can now be constantly monitored throughout each test to ensure correct displacements are reached. Load cell output can also be monitored

in real time. Motor position and load cell data is saved as a text file and can be easily accessed for future analysis. Utilizing the DAQmx feature of LabVIEW, global virtual channels can easily be configured to interchange load cells within the program. This device driver also provides a simple calibration process for the load cells. Using LabVIEW, the outlined requirements were fulfilled to create a user friendly graphical user interface (GUI) for a custom bioreactor capable of displacement control for precise loading of meniscal explants to physiological and supraphysiological strains.

This was the first study to examine the direct effect of P188 on the dynamic compression of meniscal explants. Meniscal explants were examined at 1 or 7 days after undergoing 10% or 20% strain with or without P188 treated culture media. Initial results in the first 24 hours show promising potential for P188 as a pharmaceutical intervention in meniscal tissue degradation. While cell viability was unable to return to initial physiological levels after one day, the gap between 10% and 20% strain narrowed from 21% to 8%. GAG coverage showed no changes over the seven day study. However, remodeling of meniscal tissue is poorly understood and further investigation is necessary to elucidate the relationship between mechanical overloading and GAG coverage. Congruent with the GAG coverage results, there were no changes in material properties of the meniscal explants. Again, while it is known that loss of GAG coverage results in changes in material properties of the tissue, the timeline for the changes to be enacted is unknown. P188 also showed promise in reducing nitric oxide concentration (36%) after one day in the 20% strain group, which may slow tissue degradation and apoptotic cell death. While P188 has shown promise in the initial 24 hours of application,

several avenues of research should be pursued to reveal its full potential as a pharmaceutical intervention in meniscal tissue degradation.

Future Direction

Although P188 was shown to increase cell viability within the first 24 hours of application, the overall health of these "saved" cells is unknown. While the integrity of the cell membrane may be restored, the cell's ability to function as a normal, healthy cell is unclear. To further investigate polymerase chain reaction (PCR) should be utilized to investigate cell signaling of the "saved" cells. If inflammatory markers, such as interleukin-1 alpha or tumor necrosis factor alpha, are still upregulated in these saved cells, the best course of action may be to let them go through the natural process of cell death. Healthy cells are responsible for producing the extracellular matrix (ECM), collagen and GAG, which gives the meniscus its material properties. These "saved" cells may be producing an abnormal ECM, which would change the menisci's material properties over time. Longer studies are required to explain this relationship. By extending studies to 14 or 21 days, visual changes in GAG coverage may be observed. The *in vitro* study could be further optimized by investigating varying concentrations of P188. The concentration used in this study (8 mg/ml) was optimized for articular cartilage. Meniscal tissue has a lower permeability than cartilage and higher concentrations of P188 may be necessary to maximize uptake. A previous study has shown partial meniscectomy to increase strains seen by the meniscus to 20%. However, this was a small study and biological tissue properties often vary greatly from person to person. The supraphysiological compression strain may need to be increased from 20% to 30% or 40% in order to see effects of P188. Besides further *in vitro* studies, the effect of P188 on the whole knee joint should be

investigated *in vivo*. Understanding the complete effect of P188 on the knee joint is crucial in determining its efficacy as a pharmaceutical intervention to slow tissue degradation and prevent the development of post-traumatic osteoarthritis.

CHAPTER 5: APPENDIX

5.1 Bioreactor User Manual

Bioreactor Assembly and Usage Manual

Component Connections (Assembly Overview)

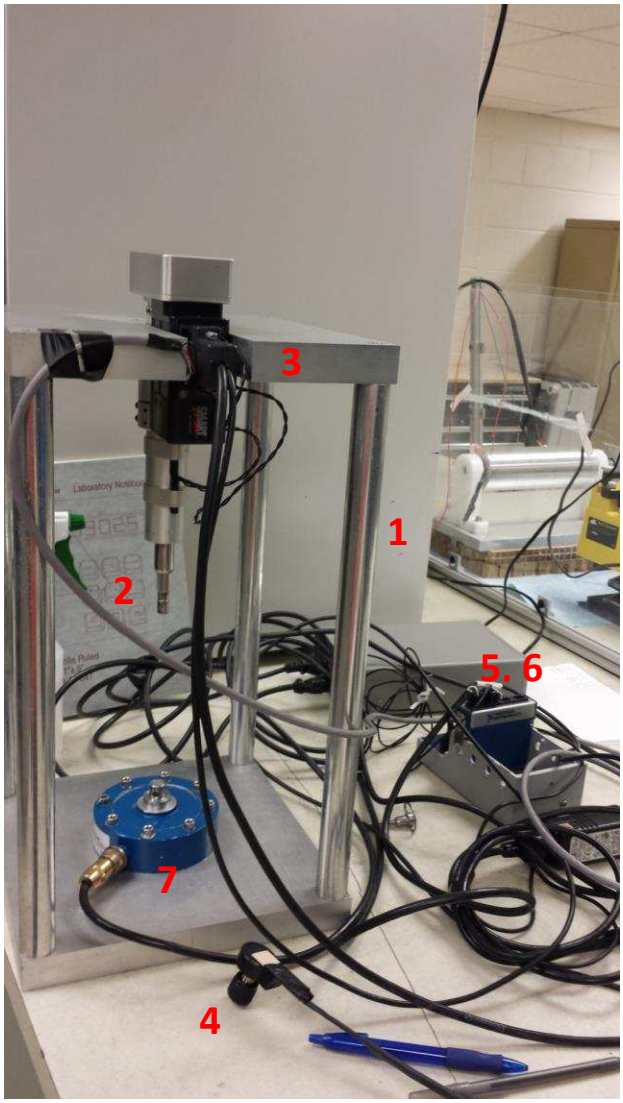

Figure 5.1.1: Bioreactor System (number labels indicate part numbers)

Table 5.1.1: Components necessary to assemble the bioreactor, with names and correlated diagram

Component Number (Diagram)	Component Name	Brief Description
1	Frame	Holds the plunger, motor, and load cell.
2	Linear Actuator	Elevates and lowers, thus compressing the specimens within the load cell.
3	SM1720 Motor	Translates Optical Rotary Encoder's digital signals to vertical movements.
4	Optical Rotary Encoder	Senses changes in light due to manual rotation, allowing the user to rotate the encoder in order to move the motor, and thus plunger up and down.
5	NI-DAQ Card and Board	Allows for signal from the load cell to be sent to the computer and understood through the NI LabVIEW program.
6	NI USB-9219 Connectors	Provides four channels of universal analog input with integrated signal conditioning.
7	1200 Precision Universal Low Profile Load Cell	Stores specimen samples, and undergoes compression and tension. Contains a strain cell which reads the changes in resistance (which then translates to changes in strains).

Parts within this manual will be referenced by both the formal name of the part, as well as the number assigned to the part.

1.) Frame

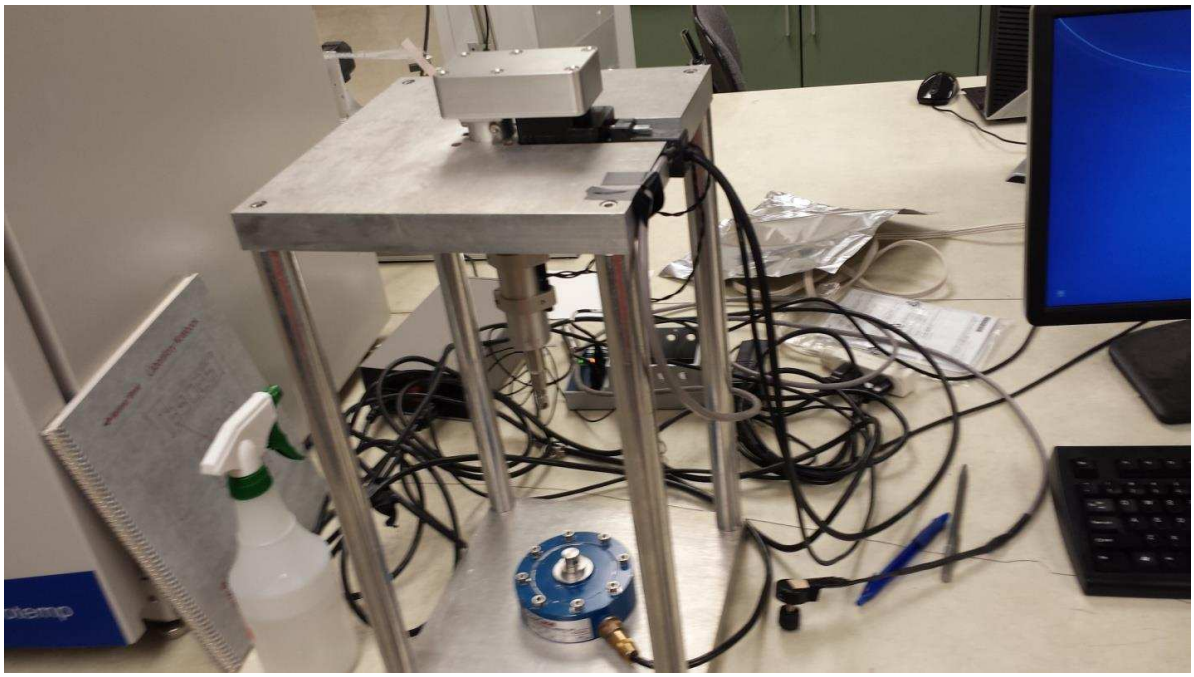

Figure 5.1.2: The Frame of the Bioreactor

The Frame (1) of the device serves the purpose of holding the Linear Actuator (2), Motor (3), and Load Cell (7), in place. The frame can be seen in Figure 2 above. The Frame is a component that was specially manufactured for the purpose of conducting material tests.

The Linear Actuator (2) can slide in and out of the frame, and is secured to the Frame (1) with bolts. The Linear Actuator (2) and Motor (3) are connected with bolts that can also be undone to allow for separation. This piece is the critical basic component for holding the entire assembly together, and allows users to conduct tension and compression tests on materials.

2.) Ultra Motion BUG Linear Actuator
(Part #4-2B.125-SM17-3.2-1NO-B/EC4)

The Linear Actuator (2) slides in and out of the frame freely once the bolts (labeled with the red circle) are undone. The Linear Actuator is then slid upward (indicated by the red arrow) to be removed from the fixture. The Linear Actuator (2) is connected to a box at the top of the fixture which contains a belt that allows the motor to translate its torsional motion to linear motion in the Actuator. The box at the top can be disassembled by removing the screws and opening the box. This is only necessary when the motor is not functioning correctly—then the belt may need to be checked.

Finally, the cords circled in blue in Figure 3, are connected to the Right and Left Limit Ports in the Smart Motor (3). This connection, and its importance, is further expanded on in the Smart Motor (3) section.

The user manual for the Linear Actuator can be seen on the following pages, and was taken from:

http://www.ultramotion.com/linear-actuators/#b-series

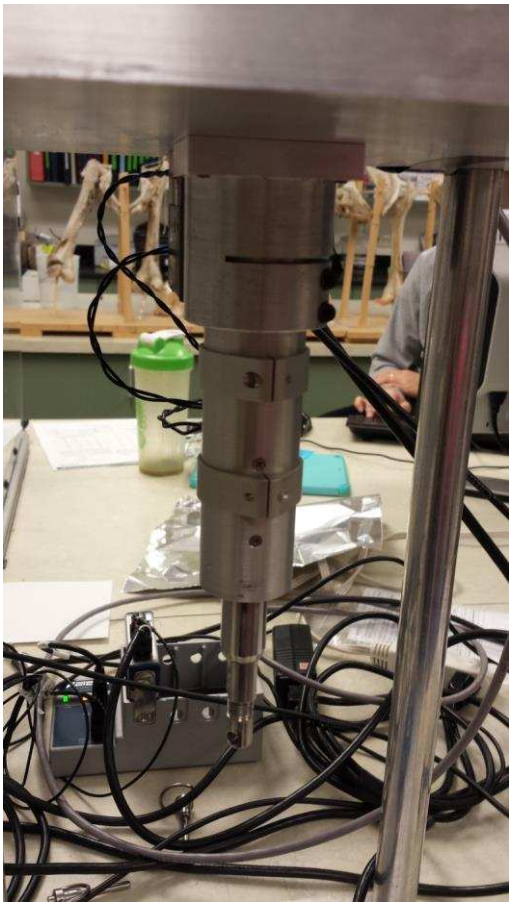

Figure 5.1.3: UltraMotion Linear Bug Actuator

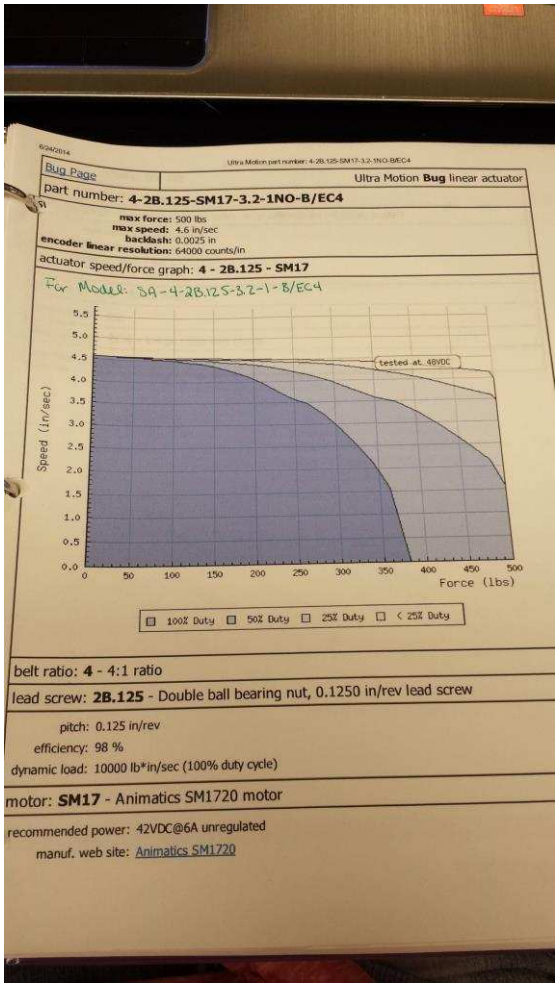

Figure 5.1.4 Specifications for Ultra Motion Bug linear actuator

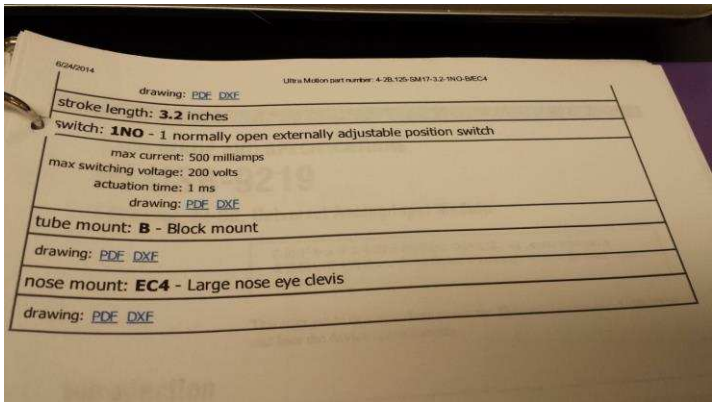

Figure 5.1.5. Specifications for Ultra Motion Bug linear actuator continued.

3.) SM1720 Smart Motor

The SM1720 Smart Motor (3) provides the mechanical power to conduct material tests on samples and can be seen in Figure 4. It functions through translating torsion forces into linear forces in the actuator. It is the central plug-in location point for many of the other parts of the device.

Located on the back of the Motor (3) are several ports that allow the connection of the Motor (3) to the computer and to the power source, Optical Rotary Encoder (4), and to the Linear Actuator (2). The instructions for connecting each of the aforementioned components can be seen on the following pages.

A diagram of the wire port configurations can be seen on the following page. The diagram represents the back of the motor while the motor is on its bottom side (which is the left side of the motor in Figure 5, located on the following page). The schematic for the motor's connection outputs was retrieved from the Animatics website at: http://www.animatics.com/download/legacy/17pin.pdf

Figure 5.1.6: SM1720 Smart Motor

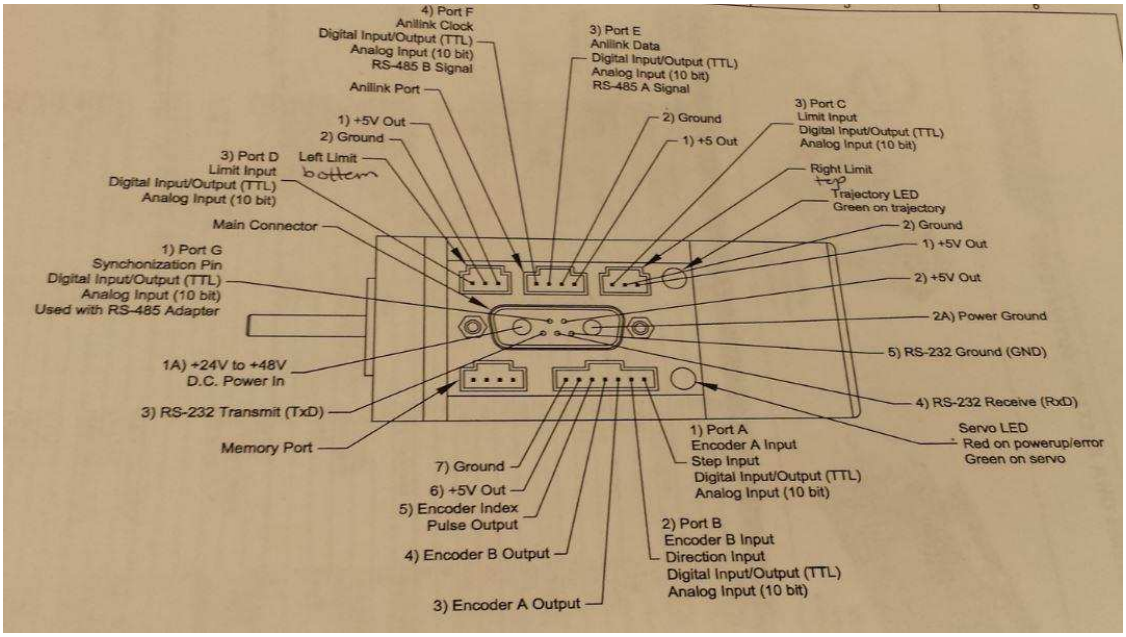

Figure 5.1.7. Pin out of Animatics Smartmotor SM1720.

Connecting the Motor (3) to the computer and power source:

In order to connect the motor to the power source and the computer, the Main Connector is used. The Main Connector plug-in is a cord that already connects both the power and computer cables. The power cord is the thicker of the two cords, while the computer cord is the thinner of the two. Connect the thicker power cord to the power outlet. Connect the thinner computer cord to the computer through the computer's serial port.

Connecting the Motor (3) to the Optical Rotary Encoder (4):

In order to connect the Optical Rotary Encoder (4) to the motor, several wires must be connected. Since the Optical Rotary Encoder (4) was attached to the motor through the soldering of the wires, the colors of the wires on the Rotary Encoder (4) end differ from the colors of the wires on the Motor's (3) end. The color changes and connection port purposes can be seen in Table 2, located below.

Table 5.1.2: Wire connection color changes and functions.

Optical Rotary Encoder Wire Color	Cable Connection to Motor Wire Color	Function of Wire
Red	Red	Red 5VDC +/- 5% @ 30 mg max
Orange	White	B Channel
Yellow	Green	A Channel
Green	Black	Ground

The Optical Encoder (4) wires must be connected to specific ports on the Motor (3). These connections, as well as the other connections necessary for the motor, can be seen in Figure 6 below.

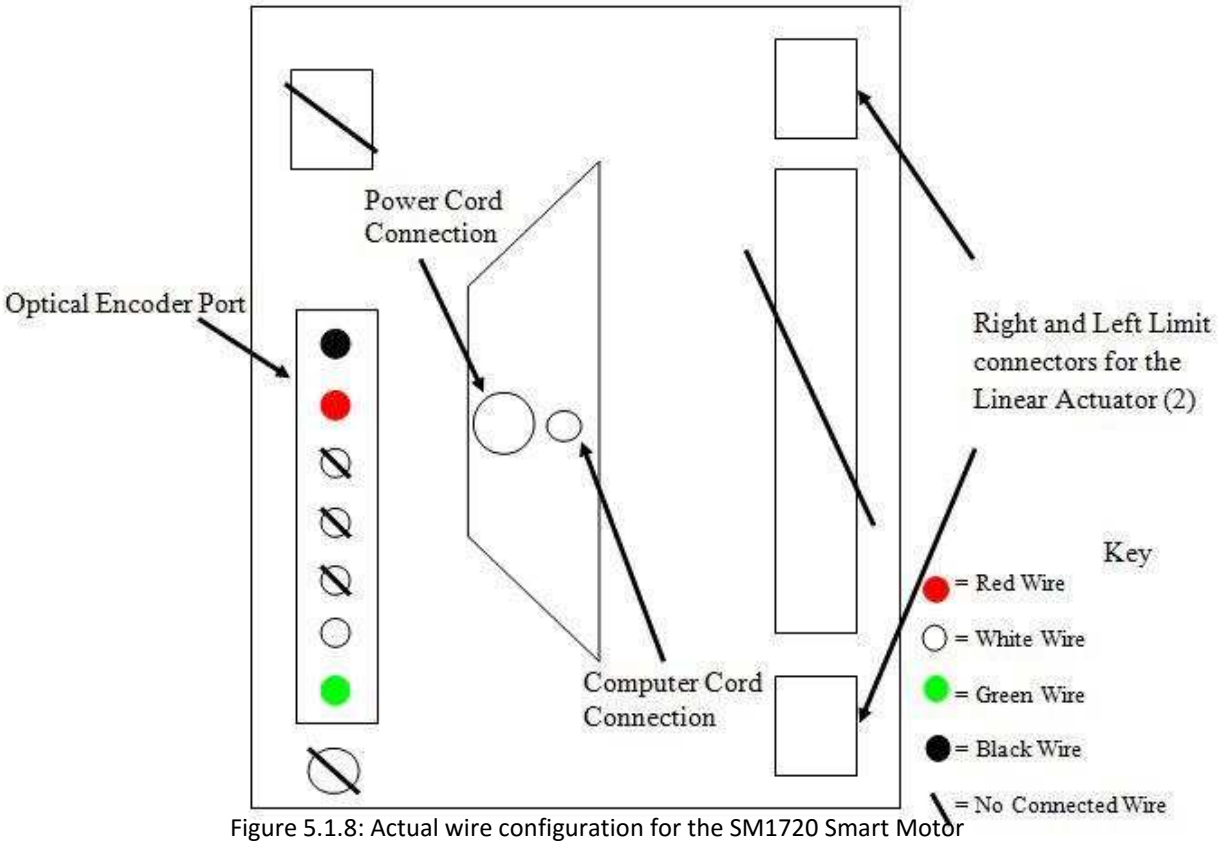

Figure 5.1.8: Actual wire configuration for the SM1720 Smart Motor

Connecting the Motor (3) to the Linear Actuator (2):

As is demonstrated in Figure 6 above, the Linear Actuator (2) is plugged into the Motor's Left and Right Limit Ports. This connection limits how far up or down the Linear Actuator (2) will move, and can be changed with programming.

The user's manual, and other critical information, CAD files, and programming software can be found at:

http://www.animatics.com/legacy-downloads.html?task=view

The user's manual can be seen on the following pages, and was also retrieved from the above website.

4.) Series 600 Optical Rotary Encoder

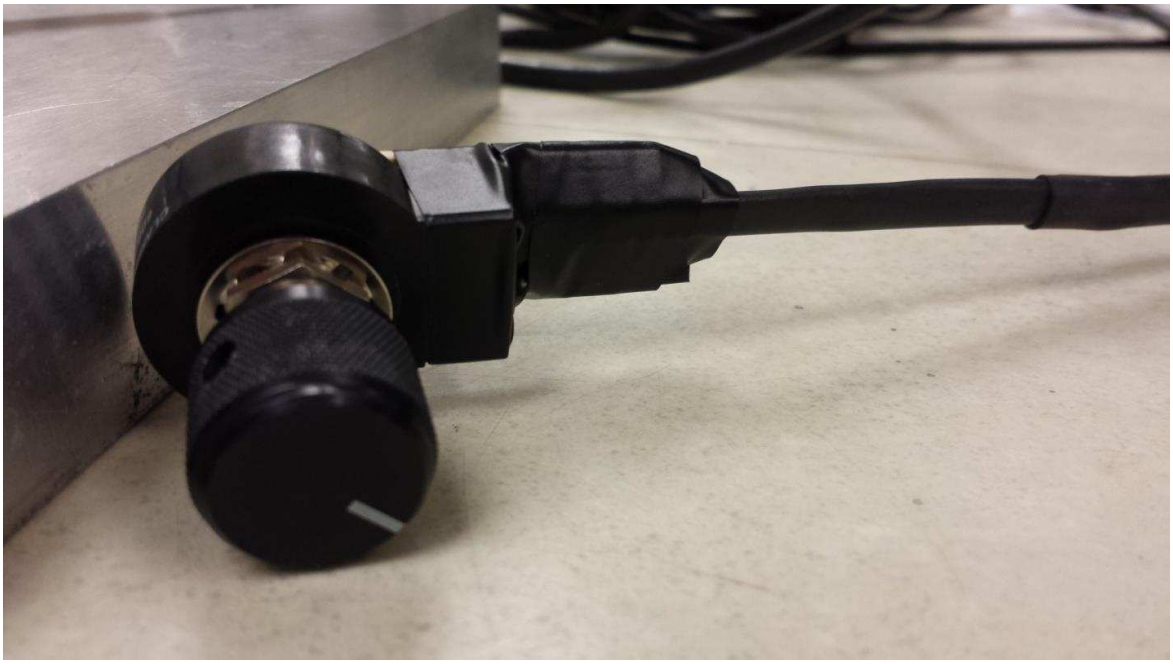

Figure 5.1.9: Series 600 Optical Rotary Encoder

The Optical Rotary Encoder (4), seen in Figure 7, allows the user to manually turn the knob on the Encoder to induce movement in the Linear Actuator (2). The Optical Rotary Encoder (4) has wiring that is soldered onto the connection cable that leads to the Motor (3) (as was stated within the Motor (3) section of the manual). Due to the soldered connection, the colors of the wires do not match at both ends, and the instructions for wiring the Optical Encoder are also included in the Smart Motor (3) section of this manual. In order to attach a new Optical Rotary Encoder, the purposes of each electrical wire must be identified and matched to the wire of the same purpose that connects to the motor.

The specifications for the optical encoder can be seen on the following pages, and was taken from State Electronic's website at:

http://www.potentiometers.com/pdf/600.pdf

Along with these specifications, more data on the configuration and installation of the optical encoder can be seen following the specifications, and was found on the Honeywell website at:

http://sensing.honeywell.com/600-series-install-50099564-a-en-final-11oct14.pdf?name=600-128-CBL

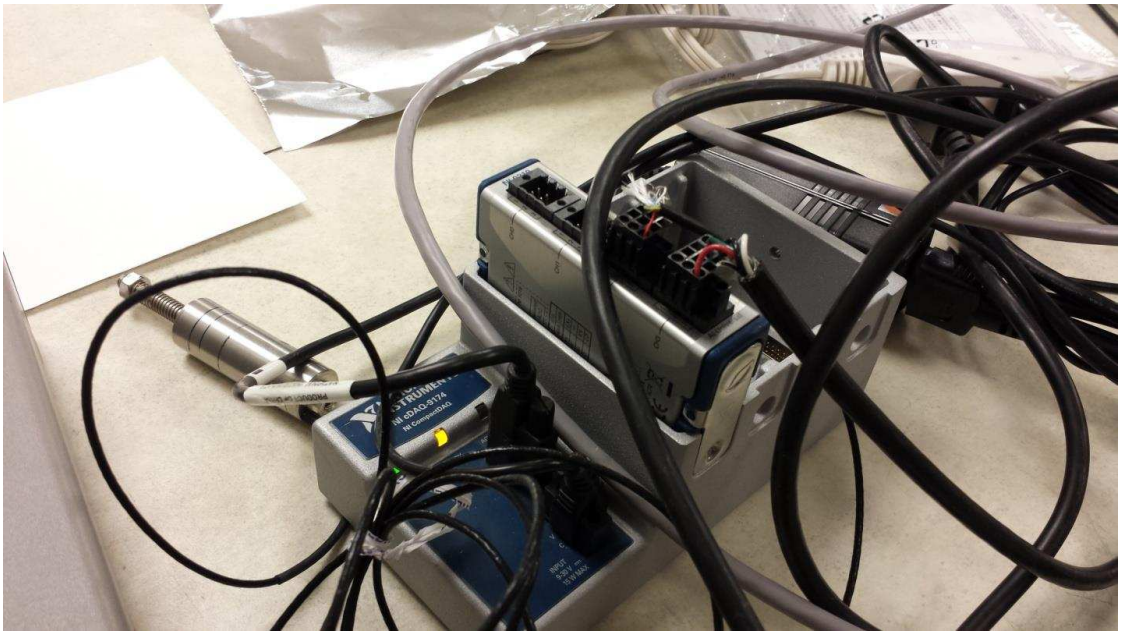

Figure 5.1.10: NI-DAQ Card and Board

5.) NI - DAQ Card and Board

The NI-DAQ Card and Board, shown in Figure 8 above, allow for the signal received from the Load Cell (7) and translated into readable data within LabVIEW. The NI-DAQ Card is inserted into the board, and allows for the NI USB Connectors (6) to be inserted into the Card. A simplified diagram of the NI-DAQ Board can be seen in Figure 9 below.

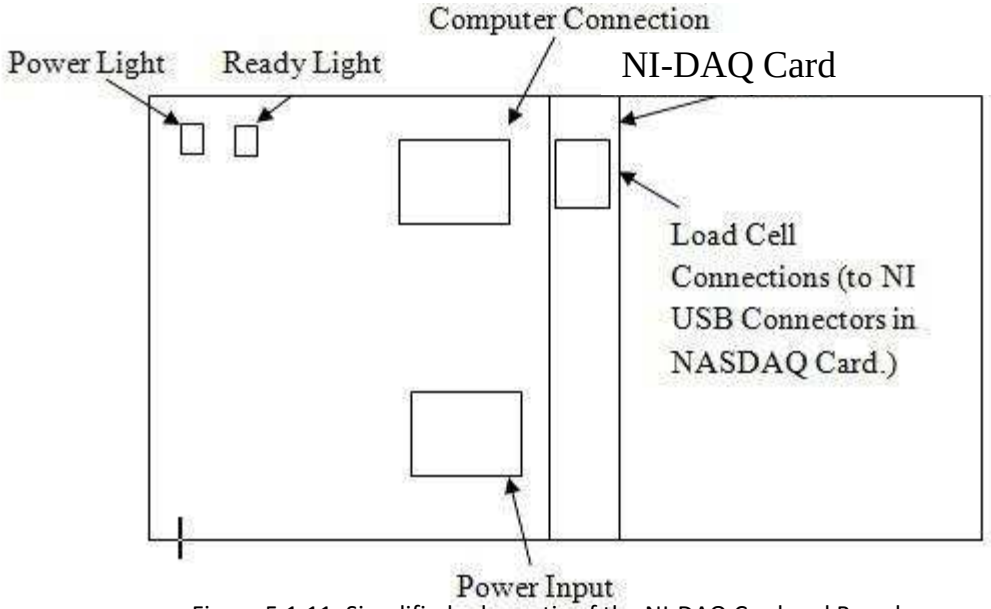

Figure 5.1.11: Simplified schematic of the NI-DAQ Card and Board Configuration

Figure 5.1.12. Close-up view of NI-USB 9219 module showing terminal connectors

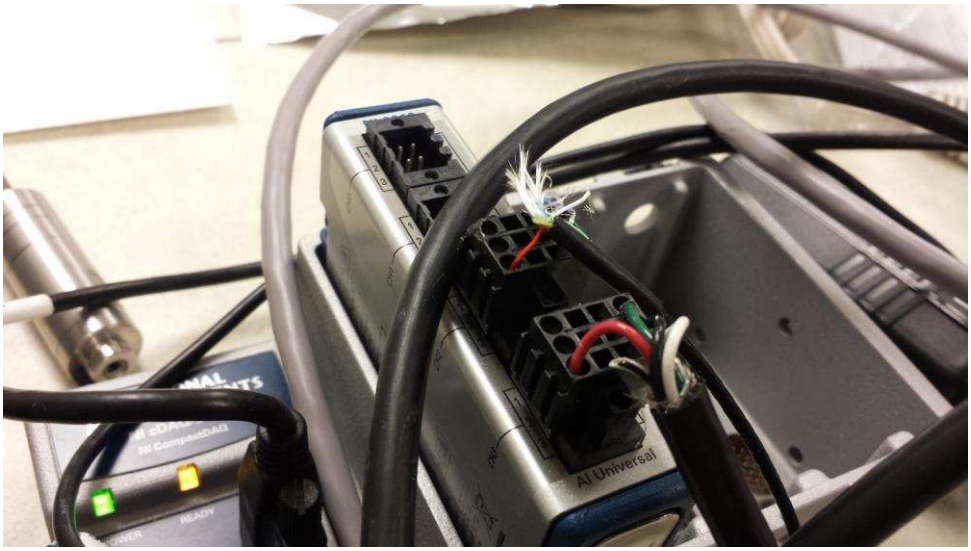

Figure 5.1.12. Close-up view of NI-USB 9219 module showing terminal connectors

6.) NI USB-9219 Connectors

In order to read data acquired from the Load Cell (7), the wire from the load cell must be connected to the NI USB-9219 Connectors (6), seen up close in Figure 10. The wires from the Load Cell (7) are connected in the manner demonstrated in Figure 11 below. The purposes of the terminals are indicated in Table 3 on the following page. In order to connect the wires to the USB-9219 Connectors (6), use a flathead screwdriver with a head smaller than 2.3 x 1.0 mm. Insert the screwdriver into the spring clamp activation slot and press the wire into the corresponding wire connecting terminal (as per the instructions provided with the USB-9219 Connectors (6)). Once the screwdriver is removed the terminal will clamp onto the inserted wire.

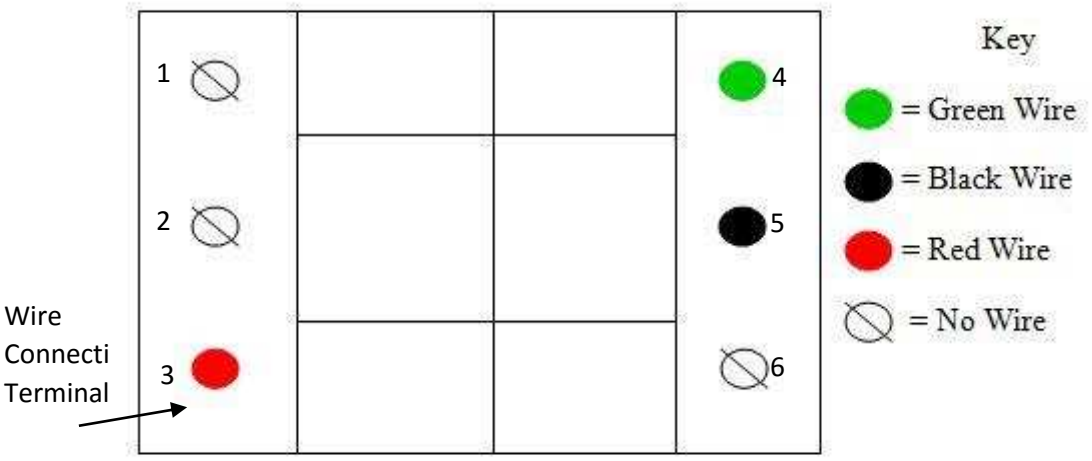

Figure 5.1.13: Wire configuration to connect the load cell to the NI USB-9219 terminal connectors

Table 5.1.3: Terminal names and descriptions for the Full Wheatstone Bridge Configuration

Terminal Number	Signal Name	Signal Description for Full Wheatstone Bridge Connection
1	T+	TEDS Data
2	T-	TEDS COM
3	EX+	Positive excitation
4	HI	Positive input signal
5	EX-	Negative excitation
6	LO	Negative input signal

The installation instructions and specifications for the NI USB-9219 Connectors can be seen on the following pages. This information was removed from the National Instruments website at:

http://www.ni.com/pdf/manuals/372407a.pdf

6.) 1200 Precision Universal Low Profile Load Cell

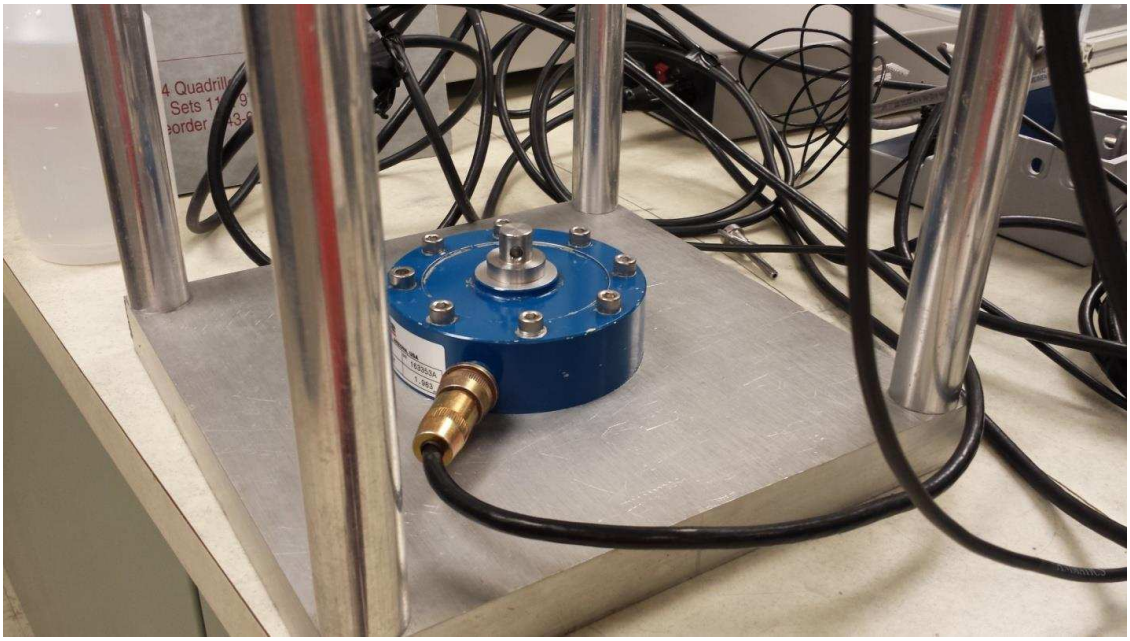

Figure 5.1.14: The load cell connected to rigid frame of bioreator

The Load Cell (7), seen in Figure 12 above, is connected to the NI USB-9219 Connectors (6) so that LabVIEW may aquire data from the tests conducted. The Load Cell (7) contains a Full-Wheatstone Bridge configuration, as is demonstrated in the wiring instructions for the NI USB-9219 Connectors (6). The load cell installation specifications and installation instructions can be seen on the following pages. This information was taken from the producer's website at:

http://www.interfaceforce.com/index.php?1200-Precision-Universal-LowProfile%99-Load-Cell-Tension-and-Compression&mod=product&show=5

SPECIFICATIONS

PARAMETERS	MODEL			
	1210	1210	1220	1232
	CAPACITY			
U.S. Models (lbf)	300, 500, 1K, 2K	5K, 10K	25K, 50K	100K
Metric Models (kN)	1.5, 2.5, 5, 10	25, 50	100, 250	450
ACCURACY – (MAX ERROR)				
Static Error Band–% FS	±0.04	±0.04	±0.04	±0.06
Nonlinearity–% FS	±0.04	±0.04	±0.04	±0.05
Hysteresis–% FS	±0.03	±0.04	±0.05	±0.06
Nonrepeatability–% RO	±0.01	±0.01	±0.01	±0.01
Creep, in 20 min–%	±0.025	±0.025	±0.025	±0.025
Side Load Sensitivity–%	±0.25	±0.25	±0.25	±0.25
Eccentric Load Sensitivity–%/in	±0.25	±0.25	±0.25	±0.25
TEMPERATURE				
Compensated Range–°F	15 to 115	15 to 115	15 to 115	15 to 115
Compensated Range–°C	-10 to 45	-10 to 45	-10 to 45	-10 to 45
Operating Range–°F	-65 to 200	-65 to 200	-65 to 200	-65 to 200
Operating Range–°C	-55 to 90	-55 to 90	-55 to 90	-55 to 90
Effect on Zero–%RO/°F – MAX	±0.0008	±0.0008	±0.0008	±0.0008
Effect on Zero–%RO/°C – MAX	±0.0015	±0.0015	±0.0015	±0.0015
Effect on Output–%RO/°F – MAX	±0.0008	±0.0008	±0.0008	±0.0008
Effect on Output–%RO/°C – MAX	±0.0015	±0.0015	±0.0015	±0.0015
ELECTRICAL				
Rated Output–mV/V (Nominal)	2.0	4.0	4.0	4.0
Excitation Voltage–VDC MAX	20	20	20	20
Bridge Resistance–Ohm (Nominal)	350	350	350	350
Zero Balance–% RO	±1.0	±1.0	±1.0	±1.0
Insulation Resistance–Megohm	5000	5000	5000	5000
MECHANICAL				
Safe Overload–% CAP	±150	±150	±150	±150
Deflection @ RO–inch	0.001	0.002	0.002	0.003
Deflection @ RO–mm	0.03	0.05	0.05	0.08
Optional Base–P/N (Metric)	B101 (M)	B102 (M)	B103 (M)	B112 (M)
Natural Frequency–kHz	3.9, 5.0, 6.9, 9.8	6.6, 9.4	6.5, 7.0	5.8
Weight–lb	1.5	3.3	9.5	26
Weight–kg	0.7	1.5	4.3	11.8
Connector	PC04E-10-6P	PC04E-10-6P	PC04E-10-6P	PC04E-10-6P
Calibration	T & C	T & C	T & C	T & C

Figure 5.1.15. Load cell specifications

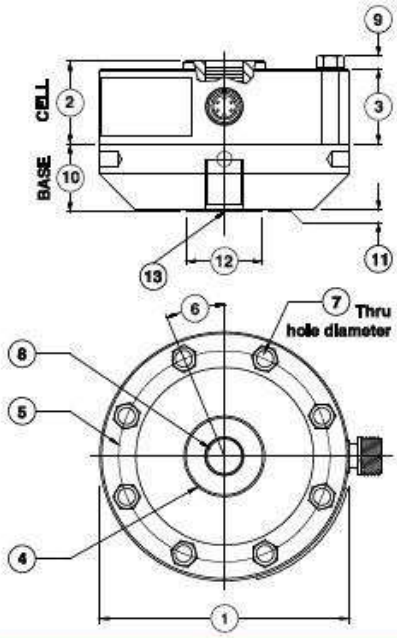

DIMENSIONS

See Drawing	MODEL					
	1210		1220		1232	
	CAPACITY					
	U.S. (lbf)	Metric (kN)	U.S. (lbf)	Metric (kN)	U.S. (lbf)	Metric (kN)
	300, 500, 1K, 2K, 5K, 10K,	1.5, 2.5, 5 10, 25, 50	25K, 50K	100, 250	100K	450
	inch	mm	inch	mm	inch	mm
(1)	4.13	104.8	6.06	153.9	8.00	203.2
(2)	1.38	34.9	1.75	44.5	2.50	63.5
(3)	1.25	31.7	1.63	41.4	2.25	57.2
(4)	1.34	34.0	2.65	67.3	3.76	95.2
(5)	3.50	88.9	5.13	130.3	6.50	165.1
(6)	22.5°	22.5°	15.0°	15.0°	11.25°	11.25°
(7)	0.28	7.10	0.41	10.4	0.53	13.5
	8 places		12 places		16 places	
(8)	5/8-18 UNF-3B	M16 x 2-4H	1 1/4-12 UNF-3B	M33 x 2-4H	1 3/4-12 UN-3B	M42 x 2-4H
	1.12 deep	28.4 deep	1.40 deep	35.6 deep	2.15 deep	54.6 deep
(9)	0.20	5.10	0.30	7.60	0.40	10.2
(10)	1.13	28.6	1.75	44.5	2.00	50.8
(11)	0.03	0.80	0.03	0.80	0.03	0.80
(12)	1.25	31.8	2.25	57.2	3.00	76.2
(13)	5/8-18 UNF-3B	M16 x 2-4H	1 1/4-12 UNF-3B	M33 x 2-4H	1 3/4-12 UNF-3B	M42 x 2-4H
	.87 deep	22.1 deep	1.40 deep	35.6 deep	1.75 deep	44.5 deep

Figure 5.1.16: Load cell dimensions

A well plate is connected, and Figure 13 shows a top view. This part is where the samples can be loaded and sealed. The configuration of the load cell is such that it allows for the samples to be completely sealed off from the environment—allowing for the user to place and maintain live tissue samples within the load cell. The samples are to be place symmetrically within the wells so that the load cell does not experience uneven strain, and thus produce faulty data. Media is to be placed into the wells as well in order to keep the tissue samples alive.

Figure 5.1.17. Top view of well plate

5.2 Standard Operating Procedures

5.2.1 Sterile Tissue Harvest

Chemicals

- Sterile PBS
- Growth Media
- 70% Isopropanol (sterilization)

Equipment

- Hood
- Scalpel blades (x per knee)
- Scalpel
- Tweezers
- Sizing apparatus
- Biopsy Punches (6 mm)
- Sterile 48 well plate
- Sterile 6 well plate
- Kimwipes
- Wire to push explants out from biopsy punch
- Cutting board

Protocol

Preparation of sterile hood

1. Wear gloves
2. Spray down interior of hood with 70% isopropanol and wipe with Kimwipe
3. Cover entire bottom surface with aluminum foil and spray with 70% isopropanol
4. Fill 4 wells with sterile PBS in 6 well plate. Use one well per meniscus. Label appropriately

Cutting Knee

1. Outside of hood, remove excess muscle and fascia without cutting into knee joint capsule.
2. Using bone saw, cut approximately 3 inches from knee joint on both sides.
3. Spray outside of joint thoroughly with 70% isopropanol and place in hood.
4. Carefully open joint capsule, taking care to avoid touching menisci. Once joint capsule is open, do not remove from hood. The knee joint within the capsule is sterile.
5. Dispose of femur.
6. Using a fresh scalpel blade and tweezers, carefully cut away menisci from the tibial plateau. Place menisci in appropriately labeled wells of PBS. Dispose of tibia.
7. Spray and wipe surface down with 70% isopropanol.
8. Moving to the clean cutting board (still in hood), carefully cut out explants using biopsy punch. Rotate the punch carefully as needed to cut through meniscus.

9. Use wire to push explant out of biopsy punch. Center the sizing apparatus on explant and push down in one fluid motion to achieve desired size.
10. Place the explant in the 48 well plate (superior surface to the top) and add 1 mL warm (37^{o}C) growth media. Place lid on plate and move to incubator.
11. Media should be changed after 24 hours.

5.2.2 P188 Media Preparation

Chemicals

- Sterile Dulbecco's Modified Eagle Medium (DMEM)
- Sterile Ham's F12 (F12)
- Penicilin/Streptomyosin
- Fetal Bovine Serum (FBS)
- 70% Isopropanol (sterilization)
- P188

Equipment

- Hood
- 2 Sterile Media Bottles
- Pipettes
- Syringe
- Sterile Filter Tip (0.45 um)
- Kimwipes
- Gloves

Protocol for Growth Media

- 1% Penicilin/Streptomyosin
- 10% FBS
- 89% DMEM:F12 [1:1]
- 8 mg/mL P188

Procedure

1. Spray down interior of hood with 70% isopropanol and wipe with KimWipe. Spray all chemical bottles and equipment with 70% isopropanol before placing in hood.
2. Loosen all caps of chemicals and sterile media bottle, but keep bottles covered with caps.
3. Without touching the containers, pipette half of DMEM:F12 into empty media bottle.
4. Add P188. Close bottle tightly and place in 37^{o}C water bath until P188 dissolves, occasionally swirling media.

5. In a new sterile bottle, add second half of DMEM:F12.
6. Attach sterile filter to syringe. Remove plunger from syringe and hold over sterile media bottle. Pour aliquots of Pen/Strep and FBS into syringe and depress plunger fully.
7. Sterile filter F12/P188 mixture using syringe into bottle containing DMEM, Pen/Strep, and FBS.
8. Aliquot into 50 mL vials.
9. If using media soon, place in water bath (37^{o}C). If finished, return to fridge.

5.2.3 Meniscus Live Dead Protocol

Equipment/Supplies:

Item	Location
Specimens (Meniscus)	Will be in test tubes from mechanical testing
Scalpel	Out from indentation testing
Tweezers	
1x PBS	
Drop cloth	
Test Tube	In Test tube drawer
Micron tube strips (2-4 depending on sample size)	On shelf above test tube drawer
Micron test tube holder	Next to micron test tube strips
Micro pipets (grey, orange, yellow)	On counter next to PBS
4 Pipet tips	In pipet drawer
Calcine	In freezer in small cylindrical container
Ethidium Bromide	
Un-subbed slides	In slides drawer
DI water	On conunter
Sharps Container	Under dissection table
Portable Hard Drive	In portable hard drive drawer

Steps for preparation

1. Place number of needed micron tubes in the micron test tube holder (x2).
2. Fill first row with PBS
3. Fill one test tube with 4 mL of PBS.
4. Remove Calcine and Ethidium Bromide from freezer so they can start to thaw
    a. Be sure to keep them unexposed to the lights
5. Turn on Incubator (~ 27 degrees)
6. Set all pipettes to appropriate measures
    a. Grey top – 1 uL
    b. Orange top – 8 uL
    c. Yellow top – 150 uL

Steps for Slicing

1. Take as thin of a slice from the middle of the explant.
2. Place thin slice in micron vial.
    i. Repeat for all specimens.

Steps for Staining

1. Turn off lights
2. Add 1uL of Calcine to test tube
3. Add 8 uL of Ethidium Bromide to same test tube
4. Vortex both test tubes to mix stain into PBD
5. Pipette 150 uL of stain into empty micron test tube rows
6. Transfer meniscal slices from PBS micron test tube rows to fluorescence rows
7. Cap the rows
8. Slightly shake rows to mix
    a. Be sure not to mix up what specimen is what
    b. Make sure all meniscal slices are at bottom of test tube
9. Place in incubator for 25 mins
10. Return Calcine and Ethidium Bromide vials to freezer
11. Remove from incubator
12. Move meniscal slices to PBS micron test tube rows
13. Place in incubator for 10 mins for a “wash”
14. Repeat wash
15. Remove from incubator
16. Turn off incubator
17. Remove slices from PBS and place on slides
18. Cover specimens with DI water to stay hydrated

Steps for Imaging

1. Turn off light
2. Turn burner on
3. Be sure in 2x
4. On Desktop open CellSense
5. Switch scope to camera
6. Will use green filter to image red (~600-900ms VERY variable)
7. Will use blue filter to image green (~1-2s but VERY variable)
8. Take photos of each image and save
    a. Ex. ZOC5_LLA_2x_G

Steps When Done Imaging

1. When all images have been taken close CellSense
2. Turn burner off
3. Place all slides in Sharps container

5.2.4 Safranin O Staining Protocol

SAFRANIN O STAINING PROTOCOL - MENISCUS

TIME: 75 MINUTES

Item	Amount
Slide Holder w/ Handle	NA
Tupperware	1
dH_20	
Tap Water	
Weigerts Iron Hematoxylin Working Solution (50:50 Parts A & B)	See Recipe
Fast Green FCF Solution	See Recipe
1%Acetic Acid Solution	See Recipe
0.1% Safranin O Solution	See Recipe
Ethanol: 95% & 100%	
Xylene	

Prepared Solutions

- Weigerts Hematoxlyin Working Solution
    1. Mix equal parts of Part A and Part B
- Fast Green FCF Solution
    1. Dissolve 0.1g fast green FCFR in 1000mL dH_20
- 1% Acetic Acid Solution
    1. Mix 10mL glacial acetic acid with 990mL dH_20
- 0.1% Safranin O Solution
    1. Dissolve 1g Safranin O in 1000mL dH_20

Methods

1. Stain with Weigert's iron hematoxylin working solution for 10 minutes
2. Wash in running tap water for 10 minutes – take care not to run faucet open too far, pressure/agitation will cause samples to come off slide
3. Stain with fast green (FCF) solution for 5 minutes
4. Rinse quickly with 1% acetic acid solution for no more than 10 – 15 seconds (~4 dips)
5. Stain in 0.1% safranin O solution for 25 minutes
6. Dehydrate and clear with 95% ethanol, absolute ethanol and xylene, using 2 changes each, for 2 minutes each

Cleanup

Weigerts, Safranin O and Fast green are saved. Filter using funnel and filter paper back into their containers (weigerts must be placed in used container as it comes separated and is mixed to activate). Acetic acid, ethanol and xylene washes are disposed of in respective labeled waste containers.

Tips

Filter and put away hematoxlyin at end of staining if you will not be staining the next day – it will degrade quickly otherwise and affect your staining!!

Replace acetic wash every other round of staining.

Trouble shooting

If slides still have stain on them, plunge slide holder up and down during the acetic acid wash and ethanol/xylene clearings.

If samples are falling off, relax slides additional times before staining, review slicing methods – if slices are not smooth and uniform they come off easier.

Weigerts solution once mixed will last approx. 3 months

Results

-GAGs: red

-Nuclei: black

-Cytoplasm: gray-green

-Cartilage, mucin, mast cell granules: orange-red

5.2.5 Live Dead Image Analysis Protocol

Image J and Cell C steps can be performed independent of each other

Image J

- Open Image J
  - Desktop -> Fiji-win64 file -> Fiji.app -> Image J-win64.exe -> Run
- Calibration Image
  - Drag and drop from Computer -> Kate -> LiveDead -> Sheep -> Live dead calibration
  - Using straight line tool draw line on calibration image
  - Analyze -> Set scale -> Type in known distance & unit length -> Global -> OK
- Import Image
  - Drag and drop from Computer -> Kate -> LiveDead -> Sheep -> Specific File of interest

- Trim Image
    - Using freehand selection tool outline image (remove outer edge and synovium)
    - Edit -> Clear Outside
    - Flood Fill Tool -> click on white background
- Save new image
    - File -> Save as -> Tiff -> label and save in appropriate location

Cell C

- Open Cell C
    - Desktop -> Cell C -> cellc.exe
- Remove save options
    - Save options -> deselect both save options
- Import Image
    - File -> Open -> Image for total cell count (Figure 1)
    - Computer -> Kate -> LiveDead -> Sheep Dead -> Specific File of interest (the trimmed file created in Image J)
- Adjustments
    - Automatic intsity threshold (Figure 1)
        - Adjustthr – > adjust threshold bar (adjust to match) -> Ok
    - Automatic removal of over/undersized cells
        - Remove objects smaller than: 0
        - Remove objects larger than: 300
    - Divide cell clusters into single cells : 0.9
    - Cluster division algorithm: Cell intensity
    - Type of Image: Fluorescence microscopy
- Analyze and Save Data
    - Click Analyze
    - Save “number of cells value
        - Computer -> Kate -> LiveDead -> Sheep -> Analysis -> Type in value where appropriate

5.2.6 GAG Analysis Protocol

Image J

- Open Image J
    - Desktop -> Fiji-win64 file -> Fiji.app -> Image J-win64.exe -> Run
- Calibration Image
    - Drag and drop from Computer -> Kate -> GAG -> Sheep -> Study of Interest -> Calibration bright field
    - Using straight line tool draw line on calibration image
    - Analyze -> Set scale -> Type in known distance & unit length -> Global -> OK
- Import Image
    - May need to stitch images -> see next step

    - Drag and drop from Computer -> Kate -> GAG -> Sheep -> Study of Interest -> Specific File of interest
- Stitch Image (two options use Mosaic J whenever possible if blurry then pairwise sitching)
    - Mosaic J: Plugins -> Stitching -> Mosaic J
        - File -> Open Image/Open Image Sequence
        - Click on images in lower bar to bring them into working plane -> Align images
        - File -> Save as - > file name_Full -> may have to enable global scale & disable messages
    - Pairwise stitching: Drag and drop two images into Fiji (see "Import Image")
        - Plugins -> Stitching -> Pairwise stitching
        - Window will appear with two image titles -> Ok -> linear blending -> Ok -> stitched image appears
        - Image -> Type -> RGB -> RGB version appears -> File -> Save as -> file name_Full
- Trim Image
    - Import filename_Full image if not already open
    - Using freehand selection tool outline image (remove outer synovium and background)
    - Edit -> Clear Outside
    - File -> save as -> file name_Full_Trimmed

- Color Deconvelution
    - Import filename_Full_Trimmed image if not already open
    - Image -> Color -> Color Deconvelution
    - Color Deconvelution window will appear -> From ROI -> Ok
    - Ok -> select red stain -> Ok -> select blue stain -> Ok -> select backround stain
    - Delete image 3 -> Save image 2 as filename_Full_Trimmed_FG -> Save image 1 as filename_Full_Trimmed_SafO

- Thresholing SafO image
    - Import filename_Full_Trimmed_SafO image if not already open
    - Image -> Adjust -> Threshold -> Adjust to match image -> Apply

- Analyzing SafO image particles
    - Analyze -> Analyze Particles -> "0-Infinity""0-1""nothing" -> OK
    - File -> save as -> file name_Results_SafO

- Thresholing Full image
    - Import filename_Full_Trimmed image if not already open
    - Image -> Type -> 8Bit
    - Image -> Adjust -> Threshold -> Adjust to cover full image -> Apply

- Analyzing Full image particles
    - Analyze -> Analyze Particles -> “0-Infinity””0-1””nothing” -> OK
    - File -> save as -> file name_Results

Excell

- Open excel files (…Results and ….Results_SafO)
- Sum all areas (column B)
- Add totals to master Excell file for ACLF ACLT GAG Results
    - Be sure to add to All working as well as corresponding individual sheet

5.2.7 Nitric Oxide Assay Protocol

Cayman Chemical Nitrate/Nitrite Colorimetric Assay Kit

1. **All tissue culture medium must be filtered before performing assay.**
    a. Amicon Ultra – 0.5mL Centrifugal Filters 10,000 NMWL (10k)
2. Reconstitute all reagents as directed by kit booklet. Storage and stability information can be found in booklet as well. (T drive: projects: STML: Finished Protocols: Assays: Cayman NO Assay.pdf)
    a. Nitrate/Nitrite Assay Buffer
        i. Dilute to 100 mL with UltraPure water
    b. Nitrate Reductase Enzyme Preparation
        i. Reconstitute with 1.2 mL Assay Buffer. Vortex.
    c. Nitrate Reductase Cofactors Preparation
        i. Reconstitute with 1.2 mL Assay Buffer. Vortex.
    d. Nitrate Standard
        i. Reconstitute with 1.0 mL Assay Buffer. Vortex.
    e. Nitrite Standard (typically not used)
        i. Reconstitute with 1.0 mL Assay Buffer. Vortex.
    f. Griess Reagents R1 and R2
        i. Ready for use

3. Setting up the assay
    a. Example plate:
        i. S0 – Standard 0 uM
        ii. U1 – Unknown sample 1

	1	2	3	4	5	6	7	8	9	10	11	12
A	S0	S0	U1	U1	U9	U9	U17	U17	U25	U25	U33	U33
B	S1	S1	U2	U2	U10	U10	U18	U18	U26	U26	U34	U34
C	S2	S2	U3	U3	U11	U11	U19	U19	U27	U27	U35	U35
D	S3	S3	U4	U4	U12	U12	U20	U20	U28	U28	U36	U36
E	S4	S4	U5	U5	U13	U13	U21	U21	U29	U29	U37	U37
F	S5	S5	U6	U6	U14	U14	U22	U22	U30	U30	U38	U38
G	S6	S6	U7	U7	U15	U15	U23	U23	U31	U31	U39	U39
H	S7	S7	U8	U8	U16	U16	U24	U24	U32	U32	U40	U40

4. Preparation of Nitrate Standard Curve
    a. If testing tissue culture media: Add 0.9 mL filtered unconditioned media to test tube. Add 0.1 mL of Nitrate standard. Vortex. Stock standard is 200 uM. To prepare standard curve, use the following table.

Well	Nitrate Standard (uL)	Media (uL)
A1, A2	0	80
B1, B2	5	75
C1, C2	10	70
D1, D2	15	65
E1, E2	20	60
F1, F2	25	55
G1, G2	30	50
H1, H2	35	45

5. Performing the assay
    a. Add up to 80 uL of sample to wells. Final volume must be adjusted to 80 uL using Assay Buffer.
    b. Add 10 uL of Nitrate Reductase Cofactors Preparation to all wells.
    c. Add 10 uL of Nitrate Reductase Enzyme Preparation to all wells.
    d. Cover the plate and incubate at room temperature for 2 hours.
    e. Add 50 uL of Griess Reagent R1 to all wells.
    f. Add 50 uL of Griess Reagent R2 to all wells.
    g. Allow color to develop for 10 minutes at room temperature.
    h. Read the absorbance at 540 nm.

5.3 Raw Data

5.3.1 Live/Dead

Raw data from Live/Dead assay.

W = 10% strain without P188

X = 20% strain without P188

Y = 10% strain with P188

Z = 20% strain with P188

1 Day							
		LIVE	**DEAD**	**TOTAL**	**% LIVE**	**% DEAD**	**%Live Average**
W1	1R-LA	342	55	397	86	14	85
W2	2R-MA	279	208	487	57	43	57
W3	1L-LP	459	83	542	85	15	
W4	3L-LA	168	39	207	81	19	81
W1	1R-LA	310	150	460	67	33	67
W2	1L-MA	222	111	333	67	33	
W3	2R-MP	225	233	458	49	51	67
W4	2L-LP	99	18	117	85	15	
W5	3R-LA	249	43	292	85	15	85
X1	1R-LP	68	99	167	41	59	44
X2	2R-MP	444	152	596	74	26	56
X3	2L-MA	180	234	414	43	57	
X4	1L-LA	229	258	487	47	53	
X5	3L-MP	725	484	1209	60	40	60
X6	2L-MP	323	304	627	52	48	
X1	1R-LP	134	162	296	45	55	45
X3	2R-MA	325	173	498	65	35	57
X4	2L-MP	170	174	344	49	51	
X5	3R-LP	377	306	683	55	45	55
Y1	1R-MP	336	115	451	75	25	75
Y2	2R-LP	322	246	568	57	43	63
Y3	2L-LP	334	153	487	69	31	
Y4	3R-MA	327	97	424	77	23	77
Y1	1R-MP	151	129	280	54	46	69

Y2	1L-LP	338	64	402	84	16	
Y3	2R-LA	244	198	442	55	45	61
Y4	2L-MA	387	193	580	67	33	
Y5	3R-MP	246	242	488	50	50	66
Y6	3R-LA	157	34	191	82	18	
Z1	1R-MA	233	122	355	66	34	60
Z2	2R-LA	239	232	471	51	49	60
Z3	2L-LP	118	50	168	70	30	
Z4	1L-MP	144	120	264	55	45	
Z5	3R-LA	417	319	736	57	43	63
Z6	3L-MP	382	173	555	69	31	
Z1	1R-MA	285	212	497	57	43	61
Z2	1L-MP	381	207	588	65	35	
Z3	2R-LP	153	115	268	57	43	56
Z4	2L-LA	695	560	1255	55	45	
Z5	3R-MA	352	219	571	62	38	57
Z6	3R-LP	341	302	643	53	47	

7 Day							
		LIVE	**DEAD**	**TOTAL**	**% LIVE**	**% DEAD**	**%Live Average**
W1	1R-LA	431	262	693	62	38	64
W2	1L-LP	286	146	432	66	34	
W3	2L-MP	325	242	567	57	43	57
W4	3R-LA	323	271	594	54	46	54
W1	1R-LA	218	73	291	75	25	72
W2	1L-LP	380	171	551	69	31	
W3	2R-MP	423	270	693	61	39	66
W4	2L-LP	459	194	653	70	30	
W5	3R-MP	269	195	464	58	42	72
W6	3L-LA	517	79	596	87	13	
X1	1R-LP	485	244	729	67	33	62
X2	1L-MP	224	162	386	58	42	
X3	2R-LA	318	279	597	53	47	53

X4	3R-LP	489	366	855	57	43	57
X1	1R-LP	404	225	629	64	36	64
X2	1L-MP	361	199	560	64	36	
X3	2R-MA	234	225	459	51	49	51
X4	2L-LA	270	261	531	51	49	
Y1	1R-MP	254	238	492	52	48	52
Y2	2R-LP	111	209	320	35	65	61
Y3	2L-LP	513	72	585	88	12	
Y4	3L-LA	382	274	656	58	42	58
Y1	1R-MP	381	120	501	76	24	76
Y2	2R-LA	200	181	381	52	48	53
Y3	2L-MA	428	377	805	53	47	
Y4	3R-LP	190	98	288	66	34	71
Y5	3L-LP	220	88	308	71	29	
Y6	3L-MP	352	105	457	77	23	
Z1	1L-LA	285	172	457	62	38	62
Z2	2R-MA	301	128	429	70	30	70
Z3	3R-MP	344	322	666	52	48	52
Z1	1L-LA	332	168	500	66	34	66
Z2	2R-LP	519	270	789	66	34	68
Z3	2L-MA	228	100	328	70	30	
Z4	3R-LA	198	121	319	62	38	62

5.5.2 GAG Coverage

Raw data from GAG histology.

1 Day					
		Saf O	**Total**	**% GAG**	**%GAG Average**
W1	1R-LA	*	*	*	
W2	2R-MA	2316694	2908034	80	80
W3	1L-LP	2572001	5693248	45	45
W4	3L-LA	3256946	5291833	62	62
W1	1R-LA	4142789	6533091	63	62
W2	1L-MA	4498399	7529580	60	
W3	2R-MP	*	*		
W4	2L-LP	3266712	5177078	63	63

W5	3R-LA	3313606	4586028	72	41
W6	3L-MP	578599	5861466	10	
X1	1R-LP	2971834	6623793	45	28
X2	2R-MP	3428056	7995592	43	54
X3	2L-MA	1911914	3591567	53	
X4	1L-LA	882018	7860699	11	
X5	3L-LP	*	*	*	
X6	2L-MP	5951751	8915482	67	
X1	1R-LP	2781996	4843451	57	57
X2	2R-MA	6814212	8165306	83	60
X3	2L-MP	2482734	6828284	36	
X4	3R-LP	4041738	8885089	45	45
Y1	1R-MP	*	*	*	
Y2	2R-LP	6190072	8081194	77	79
Y3	2L-LA	6561506	8152479	80	
Y4	3R-MA	4561329	7059787	65	65
Y1	1R-MP	4508479	7609726	59	56
Y2	1L-LP	3845740	7411310	52	
Y3	2R-LA	4914811	7900409	62	56
Y4	2L-MA	2694229	5354238	50	
Y5	3R-MP	1296967	6258116	21	39
Y6	3R-LA	3843442	6700700	57	
Z1	1R-MA	7768579	8377710	93	73
Z2	2R-LA	4458572	6574291	68	71
Z3	2L-LP	5436170	7407971	73	
Z4	1L-MP	3894156	7229441	54	
Z5	3R-LA	4035249	7008122	58	57
Z6	3L-MP	3950685	6988681	57	
Z1	1R-MA	4972466	8064818	62	62
Z2	1L-MP	4302079	6818332	63	
Z3	2R-LP	1510598	6027659	25	33
Z4	2L-LA	2546683	6194560	41	
Z5	3R-MA	4140013	7084283	58	58
Z6	3R-LP	4016774	6865446	59	

* unable to cut good slice to analyze % GAG

7 Day					
		Saf O	**Total**	**% GAG**	**%GAG Average**

W1	1R-LA	3104995	6300035	49	68
W2	1L-LP	5659351	6571000	86	
W3	2L-MP	6183631	10051385	62	62
W4	3R-LA	6391754	8044164	79	79
W1	1R-LA	4563623	7405683	62	62
W2	1L-LP	3676339	5814371	63	
W3	2R-MP	422062	6644426	6	14
W4	2L-LP	1421076	6491715	22	
W5	3R-MP	3519617	7477378	47	65
W6	3L-LA	4786495	5789946	83	
X1	1R-LP	5462997	8333880	66	56
X2	1L-MP	4178086	8907433	47	
X3	2L-LP	*	*		
X4	3L-LA	4688611	7976832	59	59
X1	1R-LP	2963813	4239107	70	62
X2	1L-MP	2288830	4302581	53	
X3	2R-MA	4504123	6599514	68	68
X4	2L-LA	3318481	4927888	67	
Y1	1L-LA	3725467	8308863	45	45
Y2	2R-MA	1907331	8687173	22	28
Y3	3R-MP	2472334	7401190	33	52
Y4	3L-LP	5704759	8126342	70	
Y1	1R-MP	3450131	8380607	41	41
Y2	2R-LA	5440470	8681445	63	45
Y3	2L-MA	1968154	7282072	27	
Y4	3R-LP	3148512	5517303	57	53
Y5	3L-LP	4867643	6950845	70	
Y6	3L-MP	2190621	7060691	31	
Z1	1L-LA	6495262	7482301	87	87
Z2	2R-MA	4104974	8068416	51	51
Z3	3R-MP	5377354	8415631	64	56
Z4	3L-LP	3981833	8156092	49	
Z1	1L-LA	4523549	6019009	75	75
Z2	2R-LP	2867141	5960211	48	36
Z3	2L-MA	1329560	5508321	24	
Z4	3R-LA	4287649	4935224	87	87

* unable to cut good slice to analyze % GAG

5.3.3 NO Assay

Standard Curve

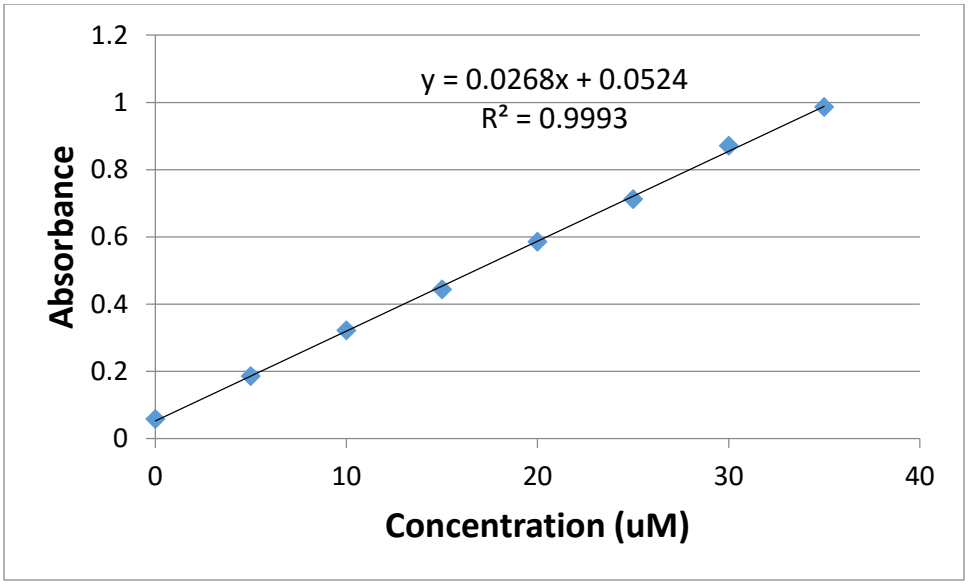

Raw Data from NO Assay.

1 Day				
Sample	**Pig**	**Absorbance**	**Concentration (uM)**	**Average Concentration**
W1	1R-LA	0.2735	8.25	8.60
W2	2R-MA	0.2535	7.503731343	7.50
W3	1L-LP	0.292	8.940298507	
W4	3L-LA	0.274	8.268656716	8.27
W1	1R-LA	0.4825	16.04850746	11.58
W2	1L-MA	0.243	7.111940299	
W3	2R-MP	0.291	8.902985075	8.11
W4	2L-LP	0.2485	7.317164179	
W5	3R-LA	0.33	10.35820896	9.63
W6	3L-MP	0.291	8.902985075	
X1	1R-LP	0.248	7.298507463	8.64
X2	2R-MP	0.2395	6.981343284	8.62
X3	2L-MA	0.2715	8.175373134	
X4	1L-LA	0.32	9.985074627	
X5	3L-LP	0.336	10.58208955	10.58
X6	2L-MP	0.3395	10.71268657	
X1	1R-LP	0.2775	8.399253731	8.40
X2	2R-MA	0.2725	8.212686567	8.69

X3	2L-MP	0.298	9.164179104	
X4	3R-LP	0.325	10.17164179	10.17
Y1	1R-MP	0.208	5.805970149	5.81
Y2	2R-LP	0.198	5.432835821	5.68
Y3	2L-LA	0.2115	5.936567164	
Y4	3R-MA	0.207	5.768656716	5.77
Y1	1R-MP	0.28	8.492537313	7.99
Y2	1L-LP	0.253	7.485074627	
Y3	2R-LA	0.238	6.925373134	8.42
Y4	2L-MA	0.318	9.910447761	
Y5	3R-MP	0.274	8.268656716	7.75
Y6	3R-LA	0.246	7.223880597	
Z1	1R-MA	0.186	4.985074627	4.73
Z2	2R-LA	0.1965	5.376865672	5.11
Z3	2L-LP	0.182	4.835820896	
Z4	1L-MP	0.1725	4.481343284	
Z5	3R-LA	0.209	5.843283582	6.06
Z6	3L-MP	0.2205	6.27238806	
Z1	1R-MA	0.2905	8.884328358	8.09
Z2	1L-MP	0.248	7.298507463	
Z3	2R-LP	0.2705	8.138059701	8.41
Z4	2L-LA	0.285	8.679104478	
Z5	3R-MA	0.2475	7.279850746	7.90
Z6	3R-LP	0.2805	8.51119403	

7 Day				
Sample	**Pig**	**Absorbance**	**Concentration (uM)**	**Average Concentration**
W1	1R-LA	0.26	7.746269	7.80
W2	1L-LP	0.263	7.858209	
W3	2L-MP	0.251	7.410448	7.41
W4	3R-LA	0.2805	8.511194	8.51
W1	1R-LA	0.357	11.36567	9.47
W2	1L-LP	0.2555	7.578358	
W3	2R-MP	0.2445	7.16791	7.07
W4	2L-LP	0.239	6.962687	
W5	3R-MP	0.227	6.514925	7.70
W6	3L-LA	0.2905	8.884328	
X1	1R-LP	0.2935	8.996269	8.75
X2	1L-MP	0.2805	8.511194	
X3	2L-LP	0.2735	8.25	8.25

X4	3L-LA	0.255	7.559701	7.56
X1	1R-LP	0.281	8.529851	8.18
X2	1L-MP	0.2625	7.839552	
X3	2R-MA	0.235	6.813433	7.01
X4	2L-LA	0.2455	7.205224	
Y1	1L-LA	0.2675	8.026119	8.03
Y2	2R-MA	0.2305	6.645522	6.65
Y3	3R-MP	0.2535	7.503731	8.36
Y4	3L-LP	0.2995	9.220149	
Y1	1R-MP	0.248	7.298507	7.30
Y2	2R-LA	0.2335	6.757463	7.28
Y3	2L-MA	0.2615	7.802239	
Y4	3R-LP	0.2245	6.421642	6.57
Y5	3L-LP	0.231	6.664179	
Y6	3L-MP	0.23	6.626866	
Z1	1L-LA	0.2735	8.25	8.25
Z2	2R-MA	0.3095	9.593284	9.59
Z3	3R-MP	0.3075	9.518657	9.29
Z4	3L-LP	0.2955	9.070896	
Z1	1L-LA	0.2905	8.884328	8.88
Z2	2R-LP	0.24	7	7.19
Z3	2L-MA	0.25	7.373134	
Z4	3R-LA	0.2425	7.093284	7.09

5.3.4 Mechanical Data

Values for “a” coefficient

7 Day				
	10 no P188	**10 P188**	**20 no P188**	**20 P188**
Day 1	74.2	40.89	201.5	328.1
Day 2	122.6	156.7	202.6	315.9
Day 3	19.27	19.27	262.2	337
Day 4	48.89	31.67	253.2	252.6
Day 5	29.74	26.22	223.5	361.4
Day 6	70.73	954.9	136.2	451
Day 7	52.23	24.85	247	252.1

Values for “b” coefficient

7 Day				
	10 no P188	**10 P188**	**20 no P188**	**20 P188**
Day 1	-0.4427	-0.2329	-0.3008	-0.2572
Day 2	-0.295	-0.06834	-0.2636	-0.2582
Day 3	-0.2259	-0.2259	-0.2275	-0.1842
Day 4	-0.1859	-0.29	-0.1336	-0.3042
Day 5	-0.3316	-0.2436	-0.304	-0.2393
Day 6	-0.2711	-0.00352	-0.3534	-0.1755
Day 7	-0.2482	-0.2377	-0.2051	-0.1774

Values for “c” coefficient

7 Day				
	10 no P188	**10 P188**	**20 no P188**	**20 P188**
Day 1	36.47	6.872	24.58	13.57
Day 2	13.41	-82.27	16.81	36.88
Day 3	3.841	3.841	9.349	-25.03
Day 4	4.655	7.67	-51.84	26.47
Day 5	12.45	6.767	12.16	7.537
Day 6	14.57	-918.2	32.11	-42.08
Day 7	2.661	4.616	-4.109	-12.41